M2 macrophages dampen *in utero* sterile inflammation to prevent preterm birth and improve neonatal outcomes

Running title: M2 Macrophages Treat Sterile Inflammation and Preterm Birth

Valeria Garcia-Flores[1,2,7], Zhenjie Liu[1,2], Roberto Romero[1,3,4], Yi Xu[1,2], Derek Miller[1,2,7], Jose Galaz[1,2,5], Andrew D. Winters[1,6], Marcelo Farias-Jofre[1,2,5], Jonathan J. Panzer[6], Kevin R. Theis[1,2,6], Nardhy Gomez-Lopez[1,2,6,7,8]

[1]Pregnancy Research Branch, Division of Obstetrics and Maternal-Fetal Medicine, Division of Intramural Research, *Eunice Kennedy Shriver* National Institute of Child Health and Human Development, National Institutes of Health, U.S. Department of Health and Human Services (NICHD/NIH/DHHS); Detroit, Michigan, and Bethesda, Maryland, USA

[2]Department of Obstetrics and Gynecology, Wayne State University School of Medicine; Detroit, Michigan, USA

[3]Department of Obstetrics and Gynecology, University of Michigan; Ann Arbor, Michigan, USA

[4]Department of Epidemiology and Biostatistics, Michigan State University; East Lansing, Michigan, USA

[5]Division of Obstetrics and Gynecology, School of Medicine, Faculty of Medicine, Pontificia Universidad Catolica de Chile; Santiago, Chile

[6]Department of Biochemistry, Microbiology, and Immunology, Wayne State University School of Medicine; Detroit, Michigan, USA

[7]Center for Reproductive Health Sciences, Department of Obstetrics and Gynecology, Washington University School of Medicine; St. Louis, Missouri, 63110, USA

[8]Department of Pathology and Immunology, Washington University School of Medicine; St. Louis, Missouri, 63110, USA

The study was conducted at the Perinatology Research Branch, NICHD/NIH/DHHS, in Detroit, Michigan; the Branch has since been renamed as the Pregnancy Research Branch, NICHD/NIH/DHHS

Correspondence: Nardhy Gomez-Lopez, PhD, Center for Reproductive Health Sciences, Department of Obstetrics and Gynecology, Washington University School of Medicine, BJC Institute of Health Rm 10618, 425 S. Euclid Ave, St. Louis, Missouri 63110, USA, Tel +1 (314) 273-8326, Email: nardhy@wustl.edu, ORCID: 0000-0002-3406-5262

Word count: 7,241

ABSTRACT

Preterm birth (PTB), often preceded by preterm labor, is a major cause of neonatal morbidity and mortality worldwide. Recent advancements in next-generation sequencing have revealed that most cases of preterm labor are associated with intra-amniotic inflammation without detectable microorganisms, a condition termed sterile intra-amniotic inflammation (SIAI). Currently, there are no established strategies to effectively treat SIAI. In this study, using an animal model of SIAI, we present mechanistic evidence demonstrating that treatment with M2 macrophages can effectively prevent PTB and mitigate adverse neonatal outcomes. We show that M2 macrophages disrupt the premature pathway of labor by suppressing inflammatory responses, including inflammasome activation, in the amniotic cavity (amniotic fluid and fetal membranes), as well as placental, fetal, and neonatal lung inflammation. Importantly, neonates exposed to SIAI exhibit compromised gut inflammation and stereotypical microbiome dysbiosis, both of which are restored by treatment with M2 macrophages. Furthermore, the long-lasting effects of M2 macrophage treatment enhance neonatal resistance to Group B *Streptococcus* infection. Collectively, our findings provide compelling evidence that M2 macrophages can serve as a cellular strategy to mitigate PTB and improve neonatal outcomes induced by *in utero* sterile inflammation.

INTRODUCTION

Preterm birth, the leading cause of neonatal morbidity and mortality worldwide[1,2], is often preceded by spontaneous preterm labor, a syndrome of multiple etiologies[3]. Among the known and proposed causes of preterm labor, intra-amniotic inflammation (IAI) is the best characterized and accounts for a large proportion of cases[3-5]. The recent incorporation of next generation sequencing in obstetrics has revealed that most cases of IAI occur in the absence of invading microbes in the amniotic cavity[6-9], resulting in the discovery of sterile intra-amniotic inflammation (SIAI). Hence, SIAI is diagnosed by elevated concentrations of inflammatory mediators such as interleukin (IL)-6 in amniotic fluid, in the absence of detectable microorganisms using culture and molecular microbiological techniques[6-10]. Importantly, SIAI has been linked to adverse short- and long-term outcomes for the offspring of women with this clinical condition[7,11]. Specifically, women with SIAI are at greater risk of having placentas affected by acute histologic chorioamnionitis[12], which is linked to the development of deleterious conditions such as bronchopulmonary dysplasia[13-15] and necrotizing enterocolitis[16,17], likely due to exposure of the fetal lungs and intestine to intra-amniotic inflammation[18-20]. Clinical studies have also shown that SIAI is associated with increased amniotic fluid concentrations of alarmins or danger signals[7,21,22], molecules released upon cellular stress or damage[23,24]. Indeed, descriptive[7,25] and mechanistic[26-28] studies have shown that the prototypical alarmin high-mobility group box-1 (HMGB1) participates in the initiation of a sterile intra-amniotic inflammatory response that leads to preterm birth. Moreover, we have elucidated key signaling pathways, such as the NLRP3 inflammasome[29], that underlie the local inflammation induced by alarmins in the amniotic cavity[12,30-32]. However, despite recent advances in the understanding of the pathophysiology of SIAI, no approved

treatments that can improve maternal and neonatal outcomes currently exist, and thus there is an urgent need for the development of effective therapeutics to combat this devastating disease.

The maternal-fetal interface hosts a notable population of macrophages displaying a homeostatic or anti-inflammatory phenotype[33-40]. During early gestation, these cells have been reported to participate in implantation and placental development as well as provide local defense against potential infection[33-38,41]. In the later stages of gestation, our recent research was the first to demonstrate that macrophages play a crucial and often overlooked role in maintaining late pregnancy and promoting optimal fetal growth[40]. Specifically, we showed that the depletion of maternal macrophages results in preterm birth, reduces neonatal survival, and causes growth restriction[40]. In this study, we also provided preliminary evidence showing that the adoptive transfer of M2-polarized macrophages prevents preterm birth induced by intra-amniotic LPS[40], suggesting that this cellular approach can serve as a feasible treatment for SIAI and its deleterious consequences.

In this study, we employed a rigorous mechanistic approach by utilizing a clinically relevant animal model of SIAI induced by the intra-amniotic injection of HMGB1 at concentrations akin to those found in amniotic fluid of women with SIAI and preterm birth[26]. We investigated the potential of adoptively transferred M2-polarized macrophages (hereafter referred to as M2 MΦ or M2 macrophages) to prevent preterm birth and reduce the adverse neonatal outcomes resulting from exposure to *in utero* sterile inflammation. Donor-recipient tracking experiments were used to characterize the migration of M2 MΦ into maternal and fetal compartments. In addition, we employed molecular approaches to investigate the inflammatory responses induced by *in utero* HMGB1 and the anti-inflammatory effect of M2 MΦ treatment in maternal and fetal tissues, including those involved in the common pathway of parturition.

Moreover, thriving neonates born to dams exposed to *in utero* HMGB1 and treated with M2 MΦ underwent gene inflammatory profiling of the lung and gut as well as gut microbiome analysis, which were compared to neonates from untreated dams. Last, to determine immunocompetence, neonates from treated and untreated dams were challenged with Group B *Streptococcus*. Collectively, our data indicate that treatment with M2 MΦ represents a novel cellular approach to prevent preterm birth and ameliorate the adverse neonatal outcomes induced by *in utero* sterile inflammation.

METHODS

Mice

C57BL/6 (strain # 000664) and B6 CD45.1 (B6.SJL-*Ptprc*^{a} *Pepc*^{b}/BoyJ; strain # 002014) mice were purchased from The Jackson Laboratory (Bar Harbor, ME, USA). Mice were housed in the animal care facility at the C.S. Mott Center for Human Growth and Development at Wayne State University (Detroit, MI, USA) under a circadian cycle (light:dark = 12:12 h). Eight- to twelve-week-old females were mated with males of proven fertility. Females were checked daily between 8 and 9 a.m. to investigate the appearance of a vaginal plug, which indicated 0.5 days *post coitum* (dpc). Plugged females were then housed separately from the male mice and their weights were monitored daily. A weight gain of ≥ 2 grams by 12.5 dpc confirmed pregnancy. Mice were randomly assigned to study groups prior to the experiments described herein. Numbers of biological replicates are indicated in each figure caption. All procedures were approved by the Institutional Animal Care and Use Committee (IACUC) at Wayne State University under Protocol Nos. A-07-03-15, 18-03-0584, and 21-04-3506.

Intra-amniotic administration of HMGB1

Ultrasound-guided intra-amniotic injection of HMGB1 was performed as previously reported[26-28]. Briefly, dams were anesthetized on 14.5 dpc by inhalation of 2% isoflurane (Fluriso™/Isoflurane, USP; VetOne, Boise, ID, USA) and 1–2 L/min of oxygen in an induction chamber, and a mixture of 1.5–2% isoflurane and 1.5–2 L/min of oxygen was used to maintain anesthesia. Mice were positioned on a heating pad and stabilized with adhesive tape, and fur was removed from the abdomen and thorax using Nair cream (Church & Dwight Co., Inc., Ewing, NJ, USA). Body temperature was detected with a rectal probe (VisualSonics, Toronto, ON, Canada)

throughout the procedure, and respiratory and heart rates were monitored by electrodes embedded in the heating pad. An ultrasound probe was fixed and mobilized with a mechanical holder, and the transducer was slowly moved toward the abdomen[42]. The ultrasound-guided intra-amniotic injection of recombinant human HMGB1 (Biolegend, San Diego, CA, USA) at a concentration of 9 ng dissolved in 100 μL of sterile 1X phosphate-buffered saline (PBS; Life Technologies, Grand Island, NY, USA) was performed in each amniotic sac using a 30G needle (BD PrecisionGlide Needle; Becton Dickinson, Franklin Lakes, NJ, USA). After ultrasound completion, mice were placed under a heat lamp for recovery defined as when the mouse resumed normal activities, such as walking and interacting with its environment, which typically occurred within 10 min after removal from anesthesia. After recovery, dams were monitored via video camera (Sony Corporation, Tokyo, Japan) to observe pregnancy and neonatal outcomes.

Isolation, differentiation, and adoptive transfer of M2-polarized macrophages

Bone marrow cells were isolated, differentiated, and adoptively transferred following a previously established protocol[40]. Briefly, bone marrow cells were collected from female mice (12-16 weeks old) and treated with red blood cell lysis buffer (Ammonium Chloride Solution; Cat# 07800, Stem Cell Technologies; Vancouver, CA). Then, cells were resuspended and cultured in Iscove's Modified Dulbecco's Media (IMDM) medium (Thermo-Fisher Scientific; Waltham, MA, USA) supplemented with 10% fetal bovine serum (FBS; Invitrogen, Carlsbad, CA, USA), 1X antibiotic-antimycotic (Cat# 15240062; Thermo-Fisher Scientific), and 10 ng/ml recombinant macrophage colony-stimulating factor (M-CSF; Cat# 576402; BioLegend, San Diego, CA, USA) for 7 days. On day 7, the culture medium was replaced with fresh IMDM medium supplemented with 10% FBS, 1X antibiotic-antimycotic, 10 ng/ml of recombinant IL-4 (Cat# 574302,

BioLegend), and 10 ng/ml of recombinant IL-13 (Cat# 575902, BioLegend). After 14-18 h, M2 MΦ were collected by washing with ice-cold phosphate-buffered saline (PBS; Fisher Scientific Bioreagents, Fair Lawn, NJ, USA or Life Technologies Limited, Pailey, UK). The purity and phenotype of macrophages after M2 polarization were routinely checked throughout the course of the study, as we have previously reported[40]. Prior to injection, the viability of M2-polarized macrophages was consistently confirmed to be >90%. Approximately 2-5 x 10^6 cells were resuspended in 100 μL 1X PBS for intravenous injection into dams on 13.5 and 14.5 dpc, prior to the administration of HMGB1 or PBS on 14.5 dpc. This timing was chosen so that the transferred M2-polarized macrophages would have sufficient time to reach key maternal and fetal tissues during the critical window of inflammation resulting in preterm birth, as previously reported[40].

Perinatal outcomes

Gestational length was calculated as the duration of time from the presence of the vaginal plug (0.5 dpc) to the detection of the first pup in the cage bedding. Preterm birth was defined as delivery occurring before 18.75 dpc based on the lowest gestational age at delivery observed in the control group. The rate of preterm birth was calculated as the proportion of females delivering preterm out of the total number of mice per group. The rate of stillbirth was defined as the proportion of delivered pups found dead among the total number of pups. The rate of neonatal mortality was defined as the proportion of pups found dead among the total number of pups. Neonatal mortality rates and weights were calculated and recorded at postnatal weeks 1, 2, and 3.

Evaluation of maternal-fetal obstetrical parameters by ultrasonography

Pregnant C57BL/6 mice were intra-amniotically injected with 9 ng of HMGB1/100 µL of PBS (or 100 µL 1x PBS as control) in each amniotic sac on 14.5 dpc and maternal-fetal obstetrical parameters were evaluated by ultrasonography (VisualSonics Inc.) 96 h after, as previously described[42-47]. The fetal heart rate and the peak systolic velocity (PSV) of the umbilical arteries of three to four fetuses from each dam were examined.

Tracking transferred M2-polarized macrophages *in vivo*

Bone marrow from B6 CD45.1 mice was collected, isolated, and differentiated into M2 MΦ as described above. Pregnant C57BL/6 recipient mice were intravenously injected with 2-5x10^6 CD45.1^+ donor M2 MΦ at 13.5 and 14.5 dpc followed by intra-amniotic injection of HMGB1 on 14.5 dpc, as described above. Mice were euthanized at 2, 6, or 12 h after intra-amniotic injection to collect the maternal blood, maternal lung, uterus, decidua, and placenta as well as the fetal membrane, fetal intestine, fetal liver, fetal liver, and amniotic fluid. Whole maternal blood (100 µL) was used directly for immunophenotyping following the procedure described below. For maternal and fetal tissues, leukocytes were isolated by following protocols adapted from[48]. Briefly, maternal and fetal tissues were gently minced using fine scissors and enzymatically digested with StemPro Accutase Cell Dissociation Reagent (Cat# A1110501, Thermo-Fisher) for 30 min at 37°C. Cells were filtered using a 100 µm cell strainer (Cat# 22-363-549, Fisher Scientific, Fair Lawn, NY, USA) followed by washing with 1X PBS prior to immunophenotyping. Immediately after isolation of leukocytes, cell pellets were re-suspended in FACS buffer and pre-incubated with rat anti-mouse CD16/CD32 Fc Block™ (Cat# 553142, clone 2.4G2; BD Bioscience, Franklin Lakes, NJ, USA) for 10 min on ice and subsequently incubated with specific fluorochrome-conjugated monoclonal anti-mouse antibodies shown in Supplementary Table 1. Cells were

acquired using the BD LSRFortessa flow cytometer (BD Biosciences) with FACSDiva 9.0 software (BD Biosciences). CountBright absolute counting beads (Thermo Fisher Scientific) were added prior to acquisition. The analysis was performed and the figures were created by using FlowJo software version 10 (FlowJo, Ashland, OR, USA).

Tissue collection from dams intra-amniotically injected with HMGB1

Dams were euthanized at 24, 48, 72, and 96 h after intra-amniotic HMGB1 injection for tissue collection. The amniotic fluid was collected from each amniotic sac and centrifuged at 1,300 x g for 5 min at 4°C. The resulting supernatants were stored at -20°C until analysis. The maternal whole blood was collected from each dam, mixed with heparin (Cat# 2106-15VL; Sigma-Aldrich, St. Louis, MO, USA), and centrifuged at 800 x g for 10 min at 4°C. Tissue collection of the uterus, decidua, placenta, fetal membrane, fetal lung, and fetal intestine was performed. The placentas and fetuses were imaged and weighed during tissue dissection. The collected tissues were snap-frozen in liquid nitrogen for immunoblotting or preserved in RNA*later* Stabilization Solution (Cat# AM7021; Invitrogen by Thermo-Fisher Scientific, Carlsbad, CA, USA), according to the manufacturer's instructions.

Determination of cytokine concentrations in amniotic fluid

Concentrations of IL-6, IL-1β, and TNF were determined in the amniotic fluid using the U-PLEX Custom Biomarker Group 1 (ms) assay (Cat# K15069M-2; Meso Scale Discovery, Rockville, MD, USA), according to the manufacturer's instructions. Plates were read using the MESO QuickPlex SQ 120 (Meso Scale Discovery) and analyte concentrations were calculated

using the Discovery Workbench software version 4.0 (Meso Scale Discovery). The sensitivities of IL-6, IL-1β, and TNF were 4.8 pg/ml, 3.1 pg/ml, and 1.3 pg/ml, respectively.

RNA isolation, cDNA synthesis, and qPCR analysis of murine tissues

Total RNA was isolated from the uterus, decidua, placenta, fetal membranes, fetal lung, fetal intestine, neonatal lung, neonatal small intestine, neonatal cecum, and neonatal colon (see below for neonatal immunocompetence experiments) using QIAshredders (Cat# 79656; Qiagen, Germantown, MD, USA), RNase-Free DNase Sets (Cat# 79254; Qiagen), and RNeasy Mini Kits (Cat# 74106; Qiagen), according to the manufacturer's instructions. The NanoDrop 8000 spectrophotometer (Thermo Scientific, Wilmington, DE, USA) and the Bioanalyzer 2100 (Agilent Technologies, Waldbronn, Germany) were used to evaluate RNA concentrations, purity, and integrity. SuperScript IV VILO Master Mix (cat# 11756050; Invitrogen by Thermo Fisher Scientific Baltics UAB, Vilnius, Lithuania) was used to synthesize complementary (c)DNA. Gene expression profiling of the tissues was performed on the BioMark System for high-throughput qPCR (Fluidigm, San Francisco, CA, USA) with the TaqMan gene expression assays (Applied Biosystems, Life Technologies Corporation, Pleasanton, CA, USA) listed in Supplementary Table 2. Negative delta cycle threshold ($-\Delta C_T$) values were determined using multiple reference genes (*Actb*, *Gapdh*, *Gusb*, and *Hsp90ab1*) averaged within each sample for contractility-associated and inflammatory genes. The $-\Delta C_T$ values were normalized by calculating the Z-score of each gene with the study groups. Heatmaps were created representing the Z-score of each $-\Delta C_T$ using GraphPad Prism (GraphPad, San Diego, CA, USA).

Protein isolation from murine tissues

Snap-frozen fetal membrane and uterus were mechanically homogenized in 1x PBS containing a complete protease inhibitor cocktail (Cat# 11836170001; Roche Applied Sciences, Mannheim, Germany) for 10 min. The resulting lysates were centrifuged at 16,100 x g (maximum speed) for 5 min at 4°C. The total protein concentrations in amniotic fluid (supernatant) and tissue lysate samples were tested by the Pierce BCA Protein Assay Kit (Cat# 23225; Pierce Biotechnology, Thermo-Fisher Scientific, Inc., Rockford, IL, USA) prior to immunoblotting. Cell lysates or concentrated culture medium from murine bone marrow-derived macrophages were utilized as positive controls for the expression of active CASP-1 and mature IL-1β, as previously described[49].

Western blotting of amniotic fluid and murine tissues

Cell lysates or culture supernatants from murine bone marrow-derived macrophages (30 μg per well; positive control), amniotic fluid (20 μg total protein per well), fetal membrane lysates (75 μg per well), and uterine tissue lysates (75 μg per well) were subjected to electrophoresis in sulfate-polyacrylamide gels (Cat# NP0336BOX; Invitrogen). The proteins were transferred onto nitrocellulose membranes (Cat# 1620145; Bio-Rad, Hercules, CA, USA), which were then submerged in 5% blotting-graded blocking solution (Cat# 1706404; Bio-Rad) for 30 min at room temperature. Next, the membranes were probed overnight at 4°C with anti-mouse CASP-1 (Cat# 14-9832-82; Thermo-Fisher Scientific) or anti-mouse mature IL-1β (Cat# 63124S; Cell Signaling Technology, Danvers, MA, USA; only for fetal membranes). After incubation with each primary antibody, membranes were incubated with HRP-conjugated anti-rat IgG (Cat# 7077S; Cell Signaling) for CASP-1 or HRP-conjugated anti-heavy chain of rabbit IgG (Cat# HRP-66467; Proteintech, Rosemont, IL, USA) for mature IL-1β for 1 h at room temperature. The ChemiGlow

West Chemiluminescence Substrate Kit (Cat# 60-12596-00; ProteinSimple, San Jose, CA, USA) was used to detect chemiluminescence signals, and corresponding images were acquired using the ChemiDoc Imaging System (Bio-Rad). The membranes that were loaded with fetal membrane and uterine tissue lysates were re-probed for 1 h at room temperature with a mouse anti-β-actin (ACTB) monoclonal antibody (Cat# A5441, Sigma-Aldrich). Then, the membranes were incubated with HRP-conjugated anti-mouse IgG (Cat# 7076S; Cell Signaling) for 30 min at room temperature. The chemiluminescence signals of the ACTB were detected as shown above. Finally, quantification was performed using ImageJ software as previously reported [49]. In short, each individual protein band was automatically quantified on the blot images. The internal control, β-actin, was used to normalize the target protein expression in each fetal membrane and uterine tissue sample for relative quantification.

Immunoprecipitation of mature IL-1β in amniotic fluid and uterine tissues

Immunoprecipitation of cleaved IL-1β from uterine tissue lysates and amniotic fluid was performed using the Pierce™ Classic IP Kit (Cat# 26146; Thermo Fisher Scientific) following the manufacturer's instructions. Amniotic fluid samples (n = 3 per study group) were pooled. Culture supernatants from murine bone marrow-derived macrophages were utilized as positive controls. Each uterine tissue lysate (1 mg protein) or pooled amniotic fluid sample (1 mg protein) was pre-cleared using the control agarose resin and incubated with rabbit anti-mouse mature IL-1β antibody overnight at 4°C to form the immune complex. Next, the immune complex was captured using Pierce Protein A/G Agarose. After several washes to remove non-bound proteins, the immune complex was eluted with sample buffer and subjected to electrophoresis in 4%–12% polyacrylamide gels followed by Western blot transfer, as described above. The blot was then

incubated with rabbit anti-mouse mature IL-1β antibody, followed by incubation with an HRP-conjugated anti-heavy chain of rabbit IgG antibody. Finally, chemiluminescence signals were detected with the ChemiGlow West Substrate Kit and images were acquired using the ChemiDoc Chemiluminescence Imaging System, and quantification was performed using ImageJ software.

Neonatal bacterial challenge and tissue collection for gene expression

Group B *Streptococcus* (GBS, CNCTC 10/84, serotype V, sequence type 26, from Dr. Thomas Hooven lab[50]) was originally isolated from a neonate with sepsis. From an overnight culture, a sub-culture was placed with fresh Tryptic Soy Broth (Cat# 211825; BD Bioscience, Franklin Lakes, NJ, USA) and grown to the logarithmic phase (OD600 0.8-0.9). Additional dilution was performed using sterile 1X PBS to reach working concentrations.

Thriving term neonates (14-16 days old) born to dams that did not receive any treatment (control) and dams injected solely with HMGB1, PBS (vehicle for M2 MΦ) followed by HMGB1, or M2 MΦ followed by HMGB1 were intraperitoneally injected with $2x10^6$ colony-forming units of GBS in 200 µL 1X sterile PBS. Survivability, body weight, and rectal temperature of the challenged neonates were checked at 4-6 h intervals throughout the daytime for 5 days. A separate cohort of neonates born to dams that received M2 MΦ or PBS followed by HMGB1 were sacrificed at 14 days of life and the lung and intestine were preserved in RNA*later* Stabilization Solution for gene expression analysis (see "**RNA isolation, cDNA synthesis, and qPCR analysis of murine tissues**" above).

Neonatal tissue collection for gut microbiome analysis

Dams underwent treatment with M2 MΦ alone, or were injected with HMGB1 and treated with vehicle or M2 MΦ as described above. A group of non-injected dams (control) was also included. There was no group-level separation of these dams; each was housed alone after receiving their respective injections. After delivery, dams were housed with their neonates. Surviving neonates were euthanized on postnatal day 14-16. Samples from the neonatal small intestine, cecum, and colon as well as environmental controls were obtained using sterile swabs (FLOQSwabs, Cat# 553C Copan Diagnostics, Murieta, CA, USA) under aseptic conditions. Each experimental group included samples obtained from neonates born to three different dams. All swab samples collected for 16S rRNA gene sequencing were stored at -80°C until DNA extractions were performed.

DNA extraction

Genomic DNA was extracted from swabs of the small intestine, cecum, and colon (n = 35 each) and negative blank DNA extraction kit controls using the DNeasy PowerLyzer Powersoil kit (Qiagen, Germantown, MD, USA), with minor modifications to the manufacturer's protocol as previously described[51-53]. All swabs were randomized across extraction runs. The purified DNA was stored at -20°C.

16s rRNA Gene Sequencing

The V4 region of the 16S rRNA gene was amplified and sequenced via the dual indexing strategy developed by Kozich et al.[54] as previously described[51-53,55], with the exception that library builds were performed using 32 cycles of PCR prior to the equimolar pooling of all sample libraries for multiplex sequencing. 16S rRNA gene sequences were clustered into amplicon sequence

variants (ASVs) defined by 100% sequence similarity using DADA2 version 1.12[56] in R version 4.2.2[57] as previously described[58], with the exception that forward and reverse reads were truncated at 240 and 215 bases, respectively. Sequences were then classified using the silva_nr_v132_train_set database with a minimum bootstrap value of 80%, and sequences that were derived from Archaea, chloroplast, Eukaryota, or mitochondria were removed.

Potential background DNA contaminant ASVs were identified using the R package decontam version 1.18.0[59] and the "IsContaminant" function. One of the 82 ASVs identified as a contaminant [Lachnospiraceae (ASV-2)] was present in > 90% of both biological and control samples, however, it had a greater mean relative abundance in biological (12.95%) than in control samples (1.77%) and was therefore not removed from the dataset. The two taxa with the highest mean prevalence and abundance in control samples that were removed from the dataset were Burkholderiaceae (ASV-42) (41.7% and 5.3%) and *Pseudomonas* (ASV-97) (50.0% and 3.8%, respectively). The mean relative abundances of these two ASVs across all biological samples were 0.0003% and 0.006%, respectively. Other ASVs removed from the dataset included taxa that have previously been reported to be contaminants in 16S rRNA gene sequencing studies (e.g., *Acinetobacter*, *Cloacibacterium*, *Corynebacterium*, *Cutibacterium*, *Escherichia*, *Halomonas*, *Pseudomonas*, *Ralstonia*, *Sphingomonas*, *Staphylococcus*, *Stenotrophomonas*, and *Xanthomonas*)[55,60-63].

After removing contaminant ASVs, all samples were normalized to 8,715 reads using the "rarefy_even_depth" function in phyloseq 1.42.0[64], resulting in 20 bacterial profiles with Good's coverage[65] values ≥ 99.68% for each of the three sample types. The final dataset contained a total of 411 ASVs. No cross-tissue comparisons were conducted.

Beta diversity

Beta diversity of bacterial profiles was characterized using the Bray-Curtis similarity index. Principal coordinate analysis (PCoA) plots were used to visualize the Bray-Curtis similarity of the sample profiles. Using nonparametric multivariate analysis of variance (NPMANOVA) as implemented in vegan 2.6.4[66], differences in bacterial community structure across treatments were evaluated for each tissue type.

Differential abundance of bacterial species

Differential abundance of the 25 most prevalent ASVs between treatment groups was independently evaluated for the small intestine, cecum, and colon datasets using Mann-Whitney U-tests with Holm's correction for multiple comparisons as implemented in R version 4.2.2. Adjusted p-values < 0.1 were considered significant.

Statistics

Statistical analyses were performed using GraphPad Prism (v9.5.0; GraphPad, San Diego, CA, US) as indicated in each figure caption. Flow cytometry analysis was performed using FlowJo software version 10. Protein expression quantification was performed using ImageJ software. To determine gene expression levels from qPCR arrays, $-\Delta C_T$ values were calculated using averaged reference genes (*Actb, Gapdh, Gusb*, and *Hsp90ab1*) within each sample. Heatmaps were created to represent the Z-scores. Microbiome data analysis was performed using R (v.4.2.2; https://www.r-project.org/), as described above. A p-value ≤ 0.05 or adjusted p-value (q-value) ≤ 0.1 was considered statistically significant.

Data availability

16S rRNA gene sequencing files and associated metadata have been uploaded to the National Center for Biotechnology Information's Sequence Read Archive (PRJNA925285). All other data are presented within the current manuscript and/or its supplementary materials.

RESULTS

Treatment with M2 macrophages prevents preterm birth and neonatal mortality induced by *in utero* exposure to HMGB1

To mimic the human disease, pregnant mice underwent an ultrasound-guided intra-amniotic injection of HMGB1 (Figure 1a) at concentrations found in women with preterm labor and SIAI[7]. The intra-amniotic delivery of HMGB1 shortened gestational length (Figure 1b), resulting in high rates of preterm birth (Figure 1c). Notably, treatment with M2 MΦ extended gestational length, preventing preterm birth (Figure 1b&c). Most preterm neonates died shortly after delivery in the HMGB1 group; yet, such an effect was rescued by treatment with M2 MΦ (Figure 1d). Consistently, neonates born to dams intra-amniotically injected with HMGB1 failed to thrive, but once again this effect was ameliorated by treatment with M2 MΦ (Figure 1e). Moreover, surviving neonates that had been exposed to *in utero* HMGB1 displayed growth restriction; however, such impairment was rescued by prenatal treatment with M2 MΦ (Figure 1f). These data indicate that M2 MΦ treatment prevents preterm birth and adverse neonatal outcomes induced by exposure to *in utero* sterile inflammation.

M2 macrophages dampen HMGB1-induced inflammation, including inflammasome activation, in the amniotic cavity

We next sought to uncover the mechanisms whereby adoptively transferred M2 MΦ were preventing adverse outcomes driven by *in utero* exposure to HMGB1. We first collected the amniotic fluid of HMGB1-injected dams at 24, 48, 72, or 96 h post-injection to evaluate the concentrations of IL-6, total IL-1β, and TNF - classic cytokines associated with SIAI[21,22] (Figure 2a). The intra-amniotic delivery of HMGB1 increased the amniotic fluid concentrations of IL-6,

the gold standard cytokine used to clinically diagnose SIAI[6,7], at 72 h post-injection (Figure 2b), approximately 24 hours before preterm delivery (Figure 1b). The concentrations of total IL-1β and TNF were not significantly affected by HMGB1 (Supplementary Figure 1). Notably, M2 MΦ treatment not only reduced amniotic fluid concentrations of IL-6 at 72 h post-injection, but also those of TNF and total IL-1β (Figure 2c&d). We then focused on the inflammasome, a key signaling pathway implicated in the intra-amniotic inflammatory response triggered by alarmins, leading to the processing of active caspase (CASP)-1 and mature IL-1β (Figure 2e), and ultimately preterm labor and birth[29,30,32,67]. The intra-amniotic delivery of HMGB1 caused an increase in active CASP-1 and mature IL-1β in amniotic fluid (Figure 2f&g). Notably, M2 MΦ treatment dampened such inflammasome activation by reducing both active CASP-1 and mature IL-1β (Figure 2h-i). These data indicate that M2 MΦ exert their homeostatic effects in the amniotic cavity by dampening the HMGB1-induced inflammatory cytokine response, including inflammasome activation.

M2 macrophages dampen inflammasome activation and regulate gene expression in the fetal membranes surrounding the amniotic cavity

The processes of term and preterm labor share a common underlying pathway including fetal membrane activation, uterine contractility, and cervical remodeling[68-71]. Such processes are also characterized by the activation of pro-inflammatory signaling networks, including inflammasome activation[72]. Indeed, our recent findings highlight the essential role of inflammasome activation in initiating labor via the common pathway, particularly evident in fetal membranes and uterine tissues during SIAI[32]. However, this mechanism does not appear to be significant in cervical tissues[32,73]. Hence, we next evaluated whether M2 MΦ treatment abrogates

inflammatory processes, including inflammasome activation in the fetal membranes (Figure 3a) and uterine tissues. Consistent with our findings in the amniotic cavity, intra-amniotic HMGB1 increased levels of active CASP-1 and mature IL-1β in the fetal membranes, indicating inflammasome activation (Figure 3b&c). Yet, M2 MΦ treatment abrogated inflammasome activation, as indicated by reduced quantities of active CASP-1 and mature IL-1β (Figure 3d&e). Gene profiling revealed that intra-amniotic HMGB1 induced the overexpression of several inflammatory genes, with only *Ccl17* significantly upregulated in the fetal membranes (Figure 3g). Conversely, M2 MΦ treatment exhibited a broad anti-inflammatory effect by downregulating the expression of *Tlr4*, *Cxcl1*, *Tnf*, and *Il1b* in the fetal membranes (Figure 3i). In the uterine tissues, intra-amniotic HMGB1 induced inflammasome activation (Supplementary Figure 2a-h), but this was not significantly reduced by treatment with M2 MΦ. However, HMGB1 did not induce an inflammatory response in uterine tissues, and treatment with M2 MΦ also did not have any effect (Supplementary Figure 3a&b). These findings suggest that mice experiencing HMGB1-induced preterm labor did not exhibit a robust inflammatory response in uterine tissues, and therefore M2 MΦ treatment did not need to suppress such a response to prevent preterm birth.

The complex pathway of parturition also involves the initiation of an immune response in the decidual tissues[3,70,74]. However, we have demonstrated that such an inflammatory response is not associated with inflammasome activation[49]. Through inflammatory gene profiling, we found that HMGB1 did not strongly induce an inflammatory response in the decidua; yet, M2 MΦ treatment downregulated several inflammatory genes (Supplementary Figure 4a&b). This finding suggests that, even in the absence of abnormal decidual inflammation, M2 MΦ treatment can effectively restrict the inflammatory response in the decidua.

Together, these findings suggest that M2 MΦ treatment primarily exerts immunomodulatory effects in the amniotic cavity and fetal membranes, offering a potential mechanism by which this cellular therapy arrests premature labor triggered by *in utero* sterile inflammation, consequently averting preterm birth.

Adoptively transferred M2 macrophages reach intrauterine compartments

Next, we evaluated whether adoptively transferred M2 MΦ were preferentially migrating to specific maternal or fetal compartments by utilizing a model wherein M2 MΦ derived from donor CD45.1$^+$ mice were transferred to recipient CD45.2$^+$ dams injected with HMGB1 (Figure 4a). Afterwards, maternal blood, maternal and fetal tissues, and amniotic fluid were collected to track the migration of transferred cells (Figure 4b). Transferred M2 MΦ retained their M2 phenotype, as previously reported[40]. Representative flow cytometry dot plots display the proportions of CD45.1$^+$ M2 MΦ detected in each maternal and fetal compartment (Figure 4c and Supplementary Figure 5a). Quantification of transferred CD45.1$^+$ M2 MΦ numbers revealed distinct kinetic patterns across the maternal and fetal compartments (Figure 4d&e and Supplementary Figure 5b). CD45.1$^+$ M2 MΦ numbers were greatest in the maternal blood and lung at 2 h post-injection, and declined to negligible counts by 12 h (Figure 4d). An opposite pattern was observed in the uterus, indicating a gradual accumulation of CD45.1$^+$ M2 MΦ over time (Figure 4d). Moreover, modest numbers of CD45.1$^+$ M2 MΦ were detected in the decidua at each time point (Figure 4d). In the fetal compartments, CD45.1$^+$ M2 MΦ were abundant in the placenta at 2 hours and declined over time (Figure 4e), following a pattern similar to that observed in maternal blood (Figure 4d), suggesting that these cells are located in the intervillous space of the placenta rather than in the parenchyma. By contrast, a small number of CD45.1$^+$ M2 MΦ

accumulated in the fetal membranes over time and could even reach the amniotic cavity (Figure 4e). CD45.1^{+} M2 MΦ were scarcely detected in the fetal intestine and lung at 2 h, and their numbers were negligible in these tissues by 6 and 12 h (Supplementary Figure 5b). The transient presence of transferred M2 MΦ is likely attributed to the exposure of the fetal lung and intestine to amniotic fluid, as evidenced by the absence of M2 MΦ in the unexposed tissue, the fetal liver, at any time point (Supplementary Figure 5b). These findings demonstrate that adoptively transferred M2 MΦ migrate to intrauterine compartments during *in utero* sterile inflammation, providing potential sites of action where such cells can exert their homeostatic effects to prevent preterm birth and improve neonatal outcomes.

M2 macrophages ameliorate placental, fetal, and neonatal lung inflammation induced by *in utero* exposure to HMGB1

Given the ability of adoptively transferred M2 MΦ to access the amniotic cavity housing the fetus and placenta (Figure 4e), our investigation focused on determining whether HMGB1 induces inflammation in the placenta and fetal lung, an organ in direct contact with the amniotic fluid. We also examined whether M2 MΦ could exert homeostatic effects in these fetal organs. The intra-amniotic delivery of HMGB1 triggered the upregulation of *Tlr4*, *Gja1*, and *Ptgs2*, along with a non-significant increase in the expression of other genes, including *Ccl17* and *Nfkb2*, in the placenta (Supplementary Figure 6a). Treatment with M2 MΦ downregulated the expression of *Ccl17* and *Nfkb2* (Supplementary Figure 6b). In the fetal lung (Figure 5a), intra-amniotic delivery of HMGB1 resulted in the upregulation of several inflammatory genes, including *Il6*, *Tnfrsf1a*, *Il33*, *Nlrp6*, and *Tlr9*, and although not statistically significant, also *Nod1* (Figure 5b&c). However, M2 MΦ treatment downregulated the expression of *Tnfrsf1a* and *Nod1* in the fetal lung (Figure

5d&e). Considering that treatment with M2 MΦ did not result in a significant suppression of the inflammatory response in the fetal lung, an organ critically linked to complications in preterm neonates[13-15], we explored whether the homeostatic effects of M2 MΦ treatment were more evident in the neonatal lung by evaluating inflammatory gene expression in this tissue. Neonates born to dams treated with M2 MΦ exhibited a diminished inflammatory profile in the neonatal lung, characterized by reduced expression of *Il6*, *Ccl2*, *Socs3*, and *Cxcl1* in comparison to offspring from untreated dams (Figure 5f&g). Collectively, these findings suggest a sustained impact of prenatal M2 MΦ treatment on the placenta as well as the fetal and neonatal lung, underscoring the homeostatic role of these cells in mitigating *in utero* sterile inflammation.

M2 macrophages regulate neonatal gut inflammation and microbiome dysbiosis resulting from *in utero* exposure to HMGB1

In addition to the lung, the fetal intestine is also exposed to the amniotic fluid. Therefore, we investigated gene expression in this organ following intra-amniotic HMGB1 injection, revealing alterations in inflammatory gene expression (Supplementary Figure 7). However, the inflammatory milieu was downregulated, suggesting that SIAI exerts different mechanisms of action across fetal organs. Since we previously showed that treatment with an anti-inflammatory drug did not exert a significant impact on the fetal intestine[75], we shifted our focus to investigate the effects of M2 MΦ treatment on the neonatal intestine (Figure 6a). Treatment with M2 MΦ boosted the neonatal gut inflammatory response dampened by *in utero* exposure to HMGB1 (Figure 6b, d, f). Specifically, M2 MΦ treatment upregulated the expression of *Aim2*, *Cd68*, *Tnf*, *Rgs4*, *Ccl5*, and *Ccl17* in the small intestine; *Casp1* and *Ccl17* in the cecum; and *Il1a*, *Cd68*, *Casp1*, *Jun*, *Kdm6b*, and *Ccl17* in the colon (Figure 6c, e, g) of neonates. These data show that

prenatal treatment with M2 MΦ enhances the neonatal gut inflammatory profile, which is otherwise suppressed by *in utero* exposure to sterile inflammation.

We recently demonstrated that *in utero* exposure to sterile inflammation leads to neonatal gut dysbiosis[75]. Therefore, we proceeded to evaluate whether treatment with M2 macrophages could mitigate this dysbiosis by performing 16S rRNA gene sequencing of the small intestine, cecum, and colon from neonates born to dams intra-amniotically injected with HMGB1 with or without M2 MΦ treatment (Figure 7a). Alpha diversity metrics of the microbiome indicated no differences in the community evenness of the small intestine, cecum, or colon between groups (data not shown). When examining beta diversity, principal coordinate analysis (PCoA) revealed that the neonatal microbiomes were strongly clustered by treatment group (Supplementary Figure 8a) and underwent consistent changes in structure (Supplementary Figure 8b). In the small intestine, M2 MΦ treatment was associated with a shift in the microbiome structure (Figure 7b&c and Supplementary Figure 8c) characterized by decreased abundance of *Rodentibacter* (ASV-5) and *Ruminiclostridium* (ASV-17) (Figure 7d). Similar patterns were also observed in the cecum (Figure 7e&f and Supplementary Figure 8d), in which a decreased abundance of *Ruminiclostridium* (ASV-17), Lachnospiraceae (ASV-24), and *Lachnoclostrium* (ASV-15) was observed alongside an increased abundance of Lachnospiraceae (ASV-39) (Figure 7g). Consistently, in the colon, the microbiome structure was altered by HMGB1 and modified by M2 MΦ treatment (Figure 7h&i and Supplementary Figure 8e), resulting in decreased abundance of *Ruminiclostridium* (ASV-17), Lachnospiraceae (ASV-24), and *Lachnoclostrium* (ASV-15) (Figure 7j). Treatment with M2 MΦ alone did not alter the alpha or beta diversity of the neonatal gut microbiome (Supplementary Figure 9a-c). Overall, these data indicate that treatment with M2 MΦ can change neonatal gut dysbiosis induced by *in utero* exposure to sterile inflammation.

M2 macrophage treatment improves neonatal ability to fight Group B *Streptococcus* infection following *in utero* exposure to HMGB1

Thus far, our research reveals that treatment with M2 MΦ enhances neonatal survival, mitigates inflammation in maternal-fetal compartments and the neonatal lung and intestine, and restores the disrupted neonatal gut microbiome following *in utero* exposure to sterile inflammation induced by HMGB1. Therefore, we last assessed whether these changes would result in improved neonatal ability to combat systemic infection with Group B *Streptococcus* (GBS). At two weeks of age, control neonates (i.e., pups born to dams without any treatment) and neonates exposed *in utero* to HMGB1 alone, HMGB1 with vehicle treatment, or HMGB1 with M2 MΦ treatment received intraperitoneal injection of GBS (Figure 8a). *In utero* exposure to HMGB1 caused low neonatal survival rates within the first five days post-GBS infection (Figure 8b). Notably, prenatal M2 MΦ treatment bolstered neonatal survival to be comparable to controls (Figure 8b), indicating improved capacity to fight GBS infection. *In utero* exposure to HMGB1 also negatively impacted neonatal weight, which was significantly reduced compared to controls at five days post-infection (Figure 8c). Prenatal M2 MΦ treatment partially rescued neonatal weight but did not fully restore it to the control trajectory (Figure 8c), a phenomenon that requires further investigation. The improved neonatal survival and growth driven by prenatal M2 MΦ treatment were accompanied by reduced incidence of hypothermia (considered the murine equivalent of fever [76,77]) upon GBS infection (Supplementary Figure 10a&b). Thus, prenatal M2 MΦ treatment bolsters immunocompetence in neonates exposed to *in utero* sterile inflammation.

DISCUSSION

In the current study, we provide mechanistic evidence for M2 macrophage treatment as a cellular therapy that can prevent preterm birth resulting from *in utero* sterile inflammation triggered by the prototypical alarmin HMGB1, which is elevated in amniotic fluid of women with SIAI[7]. The lack of knowledge regarding specific molecular targets in women with SIAI has made the investigation of useful treatment options challenging. Our current data point to several potential mechanisms whereby the adoptive transfer of M2 macrophages is preventing preterm birth. First, our prior studies have indicated that physiologic and pathologic labor is accompanied by a shift in macrophage polarization, primarily at the maternal-fetal interface, wherein a subset of such cells acquires a pro-inflammatory M1-like phenotype[39,40]. Given that adoptively transferred M2 macrophages were shown to reach the intrauterine space herein, it is possible that such cells help to maintain a predominantly homeostatic milieu in this compartment and thereby dampen inflammatory signaling that could trigger the premature onset of labor. Second, labor involves a coordinated activation across multiple maternal and fetal tissues, conventionally referred to as the common pathway of parturition[68-71], that includes modulation of processes related to contractility, tissue remodeling (e.g., matrix metalloproteinases), and inflammation[73,78-82]. Treatment with M2 macrophages may help to bolster local homeostasis, preventing the premature initiation of labor. The latter concept is supported by our prior observations that the depletion of maternal macrophages can result in preterm birth, implicating these cells in the maintenance of late gestation[40]. M2 macrophages express immunomodulatory factors, such as arginase-1 and IL-10, that can modify the tissue microenvironment and prevent local immune activation[83,84]. Indeed, in a previous study using an animal model of LPS-induced intra-amniotic inflammation, we found that treatment with M2 macrophages led to increased concentrations of IL-10 in both maternal

circulation and amniotic fluid, along with a reduction in inflammatory mediators at the maternal-fetal interface[40]. Third, we previously demonstrated that the inflammasome is a key pathway involved in premature labor induced by microbes[49,85] or alarmins[30-32,86]. As a proof of concept, we administered a specific inhibitor of the NLRP3 inflammasome (i.e., MCC950)[87] to dams injected with the alarmin S100B and observed reduced rates of preterm birth and adverse neonatal outcomes[30]. While NLRP3 inhibitors hold promise, further research is required to comprehensively assess their effects on offspring before considering their use during pregnancy. The current study demonstrates that M2 macrophages suppress inflammasome activation in the amniotic cavity, including amniotic fluid and fetal membranes, offering an alternative strategy for modulating this signaling pathway.

Sterile intra-amniotic inflammation is not only detrimental due to its short-term outcomes, such as preterm birth, but is importantly linked to long-term negative consequences for the offspring as indicated by human data[7,11] and animal studies [26-28,30,31,75,86]. Such consequences are not entirely the result of prematurity, as neonates born at term to HMGB1-injected dams still had reduced survival compared to those that received treatment with M2 macrophages. Thus, even a relatively brief exposure to *in utero* sterile inflammation imprints fetal tissue alterations that can be carried over to neonatal life, independently of gestational age at delivery. This concept is supported by previous research demonstrating that prenatal treatments or exposures during gestation can induce permanent changes in neonatal life[75,88-90]. Of interest, recent research employing a transient gestational infection model revealed the role of the IL-6/Th17 axis in augmenting offspring gut immunity, indicating that prenatal immunological events can induce long-lasting effects[89]. Transient exposure to a maternally-derived inflammatory cytokine, IL-6, was similarly explored in pregnant mice and found to result in permanent alteration of neuronal

gene programs, providing mechanistic evidence for how prenatal inflammation drives long-term changes in neonatal neurodevelopment[90]. Strikingly, in the current study, we report that prenatal treatment with M2 macrophages mitigates the negative consequences of *in utero* sterile inflammation, enhancing survival, reversing growth restriction, and overall improving neonatal infection resistance. Therefore, the current study supports two key concepts: firstly, acute insults *in utero* can disrupt developmental programming, resulting in impaired immunocompetence in the offspring, the full extent and significance of which remain poorly understood; and second, the prenatal cellular therapy using M2 macrophages demonstrated herein exerts substantial homeostatic effects, effectively countering such alterations.

Proper formation of the gut microbiota during early life is essential for the development of a healthy adult gut[91]. Indeed, multiple inflammatory, metabolic, neurologic, cardiovascular, and gastrointestinal diseases have been linked to disruption of the microbiota during early life[92]. Importantly, the risk of gut dysbiosis is increased in preterm neonates compared to those delivered at term[91], and thus the prevention or treatment of premature labor leading to preterm birth, particularly in the context of inflammatory conditions such as SIAI, is essential to ensure the development of a healthy gut microbiota and avoid long-term consequences. Several prenatal events have been studied and found to contribute to microbiota dysbiosis in human neonates, including maternal diet and antibiotic use, among others[91,93]. Specifically, the combined presence of acute histologic chorioamnionitis/funisitis was linked to altered microbial composition in neonatal fecal samples, including modified abundance of *Bacteroidetes* and *Fusobacteria*[94]. Importantly, neonates affected by acute histologic chorioamnionitis alone or acute histologic chorioamnionitis/funisitis had higher incidence of late-onset sepsis/death, thereby providing an association between microbiome alterations and short-term adverse events[94]. Consistent with these

studies, we demonstrated herein that adverse neonatal outcomes resulting from *in utero* exposure to sterile inflammation are similarly linked to alterations in gut microbiome composition, and that prenatal treatment with M2 macrophages improves these aberrations. Although the current study did not continuously examine the neonatal gut microbiome from birth to the weaning period, our results indicate that treatment with M2 macrophages promotes the proper maturation of a "healthy" gut microbiota, which can contribute to reducing disease risk in neonatal life.

It is worth acknowledging that there are inherent differences between humans and murine models. Key physiological factors such as gestational length, placental structure, immune system regulation, and hormonal regulation vary between humans and mice, as has been extensively described[95-97]. Therefore, we consider that any interventions that prove effective in murine models, such as the M2 macrophages demonstrated in the current study, require additional validation in models that more closely resemble human, such as non-human primates, to more firmly establish their clinical relevance during pregnancy.

Collectively, the data presented herein offer mechanistic evidence demonstrating that M2 macrophages represent a cellular approach to treating *in utero* sterile inflammation, thereby preventing preterm birth and adverse neonatal outcomes. Specifically, treatment with M2 macrophages mitigates inflammatory responses in the amniotic cavity, including the amniotic fluid and fetal membranes, by inhibiting inflammasome activation and halting inflammatory processes in the common pathway of labor, thereby extending gestational length and preventing preterm birth. Importantly, M2 macrophage treatment not only diminishes inflammation in the placenta as well as the fetal and neonatal lung but also enhances neonatal intestinal responses. Neonates born to dams prenatally treated with M2 macrophages demonstrate a distinct gut microbiome compared to those born from dams with *in utero* sterile inflammation, alongside an improved ability to clear

bacterial infections. In conclusion, these findings provide mechanistic evidence that M2 macrophages can serve as a cellular approach not only to prevent premature labor leading to preterm birth but also to enhance fetal and neonatal immunity following *in utero* exposure to sterile inflammation.

Acknowledgements

This research was supported by the Perinatology Research Branch, Division of Obstetrics and Maternal-Fetal Medicine, Division of Intramural Research, *Eunice Kennedy Shriver* National Institute of Child Health and Human Development, National Institutes of Health, U.S. Department of Health and Human Services (NICHD/NIH/DHHS) under Contract No. HHSN275201300006C. This research was also supported by the Wayne State University Perinatal Initiative in Maternal, Perinatal and Child Health. R.R. has contributed to this work as part of his official duties as an employee of the United States Federal Government. The funders had no role in study design, data collection and interpretation, or the decision to submit the work for publication. Figures include art created with BioRender.com

Author contributions

Conceptualization: N.G.-L.

Methodology: V.G.-F., Z.L., Y.X., N.G.-L.

Validation: V.G.-F., Z.L., Y.X., N.G.-L.

Formal analysis: V.G.-F., Z.L., R.R., Y.X., J.G., A.D.W., M.F.-J., J.J.P., N.G.-L.

Investigation: V.G.-F., Z.L., Y.X., D.M., J.G., A.D.W., M.F.-J., J.J.P., N.G.-L.

Resources: R.R., K.R.T., N.G.-L.

Data curation: V.G.-F., Z.L., Y.X., A.D.W.

Writing – original draft: V.G.-F., D.M., J.G., N.G.-L.

Writing – review & editing: V.G.-F., Z.L., R.R., Y.X., D.M., J.G., A.D.W., M.F.-J., J.J.P., K.R.T., N.G.-L.

Visualization: V.G.-F., Z.L., J.G., A.D.W., N.G.-L.

Supervision: R.R., K.R.T., N.G.-L.

Project administration: N.G.-L.

Funding acquisition: R.R., N.G.-L.

Conflict of interest

The authors have declared that no conflict of interest exists.

REFERENCES

1 Liu, L. *et al.* Global, regional, and national causes of child mortality in 2000-13, with projections to inform post-2015 priorities: an updated systematic analysis. *Lancet* **385**, 430-440 (2015). https://doi.org:10.1016/s0140-6736(14)61698-6

2 Guo, X. *et al.* A birth population-based survey of preterm morbidity and mortality by gestational age. *BMC Pregnancy Childbirth* **21**, 291 (2021). https://doi.org:10.1186/s12884-021-03726-4

3 Romero, R., Dey, S. K. & Fisher, S. J. Preterm labor: one syndrome, many causes. *Science* **345**, 760-765 (2014). https://doi.org:10.1126/science.1251816

4 Goldenberg, R. L., Culhane, J. F., Iams, J. D. & Romero, R. Epidemiology and causes of preterm birth. *Lancet* **371**, 75-84 (2008). https://doi.org:10.1016/S0140-6736(08)60074-4

5 Bastek, J. A., Gomez, L. M. & Elovitz, M. A. The role of inflammation and infection in preterm birth. *Clin Perinatol* **38**, 385-406 (2011). https://doi.org:10.1016/j.clp.2011.06.003

6 Romero, R. *et al.* A novel molecular microbiologic technique for the rapid diagnosis of microbial invasion of the amniotic cavity and intra-amniotic infection in preterm labor with intact membranes. *Am J Reprod Immunol* **71**, 330-358 (2014). https://doi.org:10.1111/aji.12189

7 Romero, R. *et al.* Prevalence and clinical significance of sterile intra-amniotic inflammation in patients with preterm labor and intact membranes. *Am J Reprod Immunol* **72**, 458-474 (2014). https://doi.org:10.1111/aji.12296

8 Romero, R. *et al.* Sterile and microbial-associated intra-amniotic inflammation in preterm prelabor rupture of membranes. *J Matern Fetal Neonatal Med* **28**, 1394-1409 (2015). https://doi.org:10.3109/14767058.2014.958463

9 Romero, R. *et al.* Sterile intra-amniotic inflammation in asymptomatic patients with a sonographic short cervix: prevalence and clinical significance. *J Matern Fetal Neonatal Med* **28**, 1343-1359 (2015). https://doi.org:10.3109/14767058.2014.954243

10 Burnham, P. *et al.* Separating the signal from the noise in metagenomic cell-free DNA sequencing. *Microbiome* **8**, 18 (2020). https://doi.org:10.1186/s40168-020-0793-4

11 Combs, C. A. *et al.* Amniotic fluid infection, inflammation, and colonization in preterm labor with intact membranes. *Am J Obstet Gynecol* **210**, 125.e121-125.e115 (2014). https://doi.org:10.1016/j.ajog.2013.11.032

12 Motomura, K. *et al.* RNA Sequencing Reveals Distinct Immune Responses in the Chorioamniotic Membranes of Women with Preterm Labor and Microbial or Sterile Intra-amniotic Inflammation. *Infect Immun* **89** (2021). https://doi.org:10.1128/IAI.00819-20

13 Lee, H. J. *et al.* Chorioamnionitis, respiratory distress syndrome and bronchopulmonary dysplasia in extremely low birth weight infants. *J Perinatol* **31**, 166-170 (2011). https://doi.org:10.1038/jp.2010.113

14 Villamor-Martinez, E. *et al.* Association of Chorioamnionitis With Bronchopulmonary Dysplasia Among Preterm Infants: A Systematic Review, Meta-analysis, and Metaregression. *JAMA Netw Open* **2**, e1914611 (2019). https://doi.org:10.1001/jamanetworkopen.2019.14611

15 Costa, S. *et al.* Effect of acute histologic chorioamnionitis on bronchopulmonary dysplasia and mortality rate among extremely low gestational age neonates: A retrospective case-control study. *Int J Gynaecol Obstet* (2023). https://doi.org:10.1002/ijgo.15290

16 Been, J. V., Lievense, S., Zimmermann, L. J., Kramer, B. W. & Wolfs, T. G. Chorioamnionitis as a risk factor for necrotizing enterocolitis: a systematic review and meta-analysis. *J Pediatr* **162**, 236-242.e232 (2013). https://doi.org:10.1016/j.jpeds.2012.07.012

17 Duci, M. *et al.* Maternal and placental risk factors associated with the development of necrotizing enterocolitis (NEC) and its severity. *J Pediatr Surg* **54**, 2099-2102 (2019). https://doi.org:10.1016/j.jpedsurg.2019.04.018

18 Kallapur, S. G., Willet, K. E., Jobe, A. H., Ikegami, M. & Bachurski, C. J. Intra-amniotic endotoxin: chorioamnionitis precedes lung maturation in preterm lambs. *Am J Physiol Lung Cell Mol Physiol* **280**, L527-536 (2001). https://doi.org:10.1152/ajplung.2001.280.3.L527

19 Wolfs, T. G. *et al.* Chorioamnionitis-induced fetal gut injury is mediated by direct gut exposure of inflammatory mediators or by lung inflammation. *Am J Physiol Gastrointest Liver Physiol* **306**, G382-393 (2014). https://doi.org:10.1152/ajpgi.00260.2013

20 Jung, E. *et al.* The fetal inflammatory response syndrome: the origins of a concept, pathophysiology, diagnosis, and obstetrical implications. *Semin Fetal Neonatal Med* **25**, 101146 (2020). https://doi.org:10.1016/j.siny.2020.101146

21 Romero, R. *et al.* Evidence of perturbations of the cytokine network in preterm labor. *Am J Obstet Gynecol* **213**, 836.e831-836.e818 (2015). https://doi.org:10.1016/j.ajog.2015.07.037

22 Bhatti, G. *et al.* Compartmentalized profiling of amniotic fluid cytokines in women with preterm labor. *PLoS One* **15**, e0227881 (2020). https://doi.org:10.1371/journal.pone.0227881

23 Matzinger, P. An innate sense of danger. *Semin Immunol* **10**, 399-415 (1998). https://doi.org:10.1006/smim.1998.0143

24 Rubartelli, A. & Lotze, M. T. Inside, outside, upside down: damage-associated molecular-pattern molecules (DAMPs) and redox. *Trends Immunol* **28**, 429-436 (2007). https://doi.org:10.1016/j.it.2007.08.004

25 Romero, R. *et al.* Damage-associated molecular patterns (DAMPs) in preterm labor with intact membranes and preterm PROM: a study of the alarmin HMGB1. *J Matern Fetal Neonatal Med* **24**, 1444-1455 (2011). https://doi.org:10.3109/14767058.2011.591460

26 Gomez-Lopez, N. *et al.* Intra-Amniotic Administration of HMGB1 Induces Spontaneous Preterm Labor and Birth. *Am J Reprod Immunol* **75**, 3-7 (2016). https://doi.org:10.1111/aji.12443

27 Galaz, J. *et al.* Betamethasone as a potential treatment for preterm birth associated with sterile intra-amniotic inflammation: a murine study. *J Perinat Med* **49**, 897-906 (2021). https://doi.org:10.1515/jpm-2021-0049

28 Galaz, J. *et al.* Clarithromycin prevents preterm birth and neonatal mortality by dampening alarmin-induced maternal-fetal inflammation in mice. *BMC Pregnancy Childbirth* **22**, 503 (2022). https://doi.org:10.1186/s12884-022-04764-2

29 Gomez-Lopez, N. *et al.* Inflammasomes: Their Role in Normal and Complicated Pregnancies. *J Immunol* **203**, 2757-2769 (2019). https://doi.org:10.4049/jimmunol.1900901

30 Gomez-Lopez, N. *et al.* Inhibition of the NLRP3 inflammasome can prevent sterile intra-amniotic inflammation, preterm labor/birth, and adverse neonatal outcomes. *Biol Reprod* **100**, 1306-1318 (2019). https://doi.org:10.1093/biolre/ioy264

31 Motomura, K. *et al.* The alarmin interleukin-1α causes preterm birth through the NLRP3 inflammasome. *Mol Hum Reprod* **26**, 712-726 (2020). https://doi.org:10.1093/molehr/gaaa054

32 Galaz, J. *et al.* A key role for NLRP3 signaling in preterm labor and birth driven by the alarmin S100B. *Transl Res* (2023). https://doi.org:10.1016/j.trsl.2023.04.004

33 Cohen, P. E., Nishimura, K., Zhu, L. & Pollard, J. W. Macrophages: important accessory cells for reproductive function. *J Leukoc Biol* **66**, 765-772 (1999). https://doi.org:10.1002/jlb.66.5.765

34 Repnik, U. *et al.* Comparison of macrophage phenotype between decidua basalis and decidua parietalis by flow cytometry. *Placenta* **29**, 405-412 (2008). https://doi.org:10.1016/j.placenta.2008.02.004

35 Houser, B. L., Tilburgs, T., Hill, J., Nicotra, M. L. & Strominger, J. L. Two unique human decidual macrophage populations. *J Immunol* **186**, 2633-2642 (2011). https://doi.org:10.4049/jimmunol.1003153

36 Svensson, J. *et al.* Macrophages at the fetal-maternal interface express markers of alternative activation and are induced by M-CSF and IL-10. *J Immunol* **187**, 3671-3682 (2011). https://doi.org:10.4049/jimmunol.1100130

37 Care, A. S. *et al.* Macrophages regulate corpus luteum development during embryo implantation in mice. *J Clin Invest* **123**, 3472-3487 (2013). https://doi.org:10.1172/JCI60561

38 Svensson-Arvelund, J. *et al.* The human fetal placenta promotes tolerance against the semiallogeneic fetus by inducing regulatory T cells and homeostatic M2 macrophages. *J Immunol* **194**, 1534-1544 (2015). https://doi.org:10.4049/jimmunol.1401536

39 Xu, Y. *et al.* An M1-like Macrophage Polarization in Decidual Tissue during Spontaneous Preterm Labor That Is Attenuated by Rosiglitazone Treatment. *J Immunol* **196**, 2476-2491 (2016). https://doi.org:10.4049/jimmunol.1502055

40 Gomez-Lopez, N. *et al.* Macrophages exert homeostatic actions in pregnancy to protect against preterm birth and fetal inflammatory injury. *JCI Insight* **6** (2021). https://doi.org:10.1172/jci.insight.146089

41 Qiu, X., Zhu, L. & Pollard, J. W. Colony-stimulating factor-1-dependent macrophage functions regulate the maternal decidua immune responses against Listeria monocytogenes infections during early gestation in mice. *Infect Immun* **77**, 85-97 (2009). https://doi.org:10.1128/iai.01022-08

42 Galaz, J. *et al.* A Protocol for Evaluating Vital Signs and Maternal-Fetal Parameters Using High-Resolution Ultrasound in Pregnant Mice. *STAR Protoc* **1**, 100134 (2020). https://doi.org:10.1016/j.xpro.2020.100134

43 Gomez-Lopez, N. *et al.* In vivo T-cell activation by a monoclonal alphaCD3epsilon antibody induces preterm labor and birth. *Am J Reprod Immunol* **76**, 386-390 (2016). https://doi.org:10.1111/aji.12562

44 St Louis, D. *et al.* Invariant NKT Cell Activation Induces Late Preterm Birth That Is Attenuated by Rosiglitazone. *J Immunol* **196**, 1044-1059 (2016). https://doi.org:10.4049/jimmunol.1501962

45 Meyer, N., Schuler, T. & Zenclussen, A. C. High Frequency Ultrasound for the Analysis of Fetal and Placental Development In Vivo. *J Vis Exp* (2018). https://doi.org:10.3791/58616

46 Arenas-Hernandez, M. *et al.* Effector and Activated T Cells Induce Preterm Labor and Birth That Is Prevented by Treatment with Progesterone. *J Immunol* **202**, 2585-2608 (2019). https://doi.org:10.4049/jimmunol.1801350

47 Gomez-Lopez, N. *et al.* Regulatory T Cells Play a Role in a Subset of Idiopathic Preterm Labor/Birth and Adverse Neonatal Outcomes. *Cell Rep* **32**, 107874 (2020). https://doi.org:10.1016/j.celrep.2020.107874

48 Arenas-Hernandez, M., Sanchez-Rodriguez, E. N., Mial, T. N., Robertson, S. A. & Gomez-Lopez, N. Isolation of Leukocytes from the Murine Tissues at the Maternal-Fetal Interface. *J Vis Exp*, e52866 (2015). https://doi.org:10.3791/52866

49 Motomura, K. *et al.* Fetal and maternal NLRP3 signaling is required for preterm labor and birth. *JCI Insight* **7** (2022). https://doi.org:10.1172/jci.insight.158238

50 Hooven, T. A. *et al.* Complete Genome Sequence of Streptococcus agalactiae CNCTC 10/84, a Hypervirulent Sequence Type 26 Strain. *Genome Announc* **2** (2014). https://doi.org:10.1128/genomeA.01338-14

51 Theis, K. R. *et al.* No Consistent Evidence for Microbiota in Murine Placental and Fetal Tissues. *mSphere* **5** (2020). https://doi.org:10.1128/mSphere.00933-19

52 Theis, K. R., Romero, R., Winters, A. D., Jobe, A. H. & Gomez-Lopez, N. Lack of Evidence for Microbiota in the Placental and Fetal Tissues of Rhesus Macaques. *mSphere* **5** (2020). https://doi.org:10.1128/mSphere.00210-20

53 Winters, A. D. *et al.* Does the Amniotic Fluid of Mice Contain a Viable Microbiota? *Front Immunol* **13**, 820366 (2022). https://doi.org:10.3389/fimmu.2022.820366

54 Kozich, J. J., Westcott, S. L., Baxter, N. T., Highlander, S. K. & Schloss, P. D. Development of a dual-index sequencing strategy and curation pipeline for analyzing amplicon sequence data on the MiSeq Illumina sequencing platform. *Appl Environ Microbiol* **79**, 5112-5120 (2013). https://doi.org:10.1128/aem.01043-13

55 Winters, A. D. *et al.* Does the endometrial cavity have a molecular microbial signature? *Sci Rep* **9**, 9905 (2019). https://doi.org:10.1038/s41598-019-46173-0

56 Callahan, B. J. *et al.* DADA2: High-resolution sample inference from Illumina amplicon data. *Nat Methods* **13**, 581-583 (2016). https://doi.org:10.1038/nmeth.3869

57 Team, R. C. R: A language and environment for statistical computing. (2013).

58 Romero, R. *et al.* The vaginal microbiota in early pregnancy identifies a subset of women at risk for early preterm prelabor rupture of membranes and preterm birth. *Research Square* (2022). https://doi.org:https://doi.org/10.21203/rs.3.rs-2359402/v1

59 Davis, N. M., Proctor, D. M., Holmes, S. P., Relman, D. A. & Callahan, B. J. Simple statistical identification and removal of contaminant sequences in marker-gene and metagenomics data. *Microbiome* **6**, 226 (2018). https://doi.org:10.1186/s40168-018-0605-2

60 Salter, S. J. *et al.* Reagent and laboratory contamination can critically impact sequence-based microbiome analyses. *BMC Biol* **12**, 87 (2014). https://doi.org:10.1186/s12915-014-0087-z

61 Glassing, A., Dowd, S. E., Galandiuk, S., Davis, B. & Chiodini, R. J. Inherent bacterial DNA contamination of extraction and sequencing reagents may affect interpretation of microbiota in low bacterial biomass samples. *Gut Pathog* **8**, 24 (2016). https://doi.org:10.1186/s13099-016-0103-7

62 Eisenhofer, R. *et al.* Contamination in Low Microbial Biomass Microbiome Studies: Issues and Recommendations. *Trends Microbiol* **27**, 105-117 (2019). https://doi.org:10.1016/j.tim.2018.11.003

63 Karstens, L. *et al.* Controlling for Contaminants in Low-Biomass 16S rRNA Gene Sequencing Experiments. *mSystems* **4** (2019). https://doi.org:10.1128/mSystems.00290-19

64 McMurdie, P. J. & Holmes, S. phyloseq: an R package for reproducible interactive analysis and graphics of microbiome census data. *PLoS One* **8**, e61217 (2013). https://doi.org:10.1371/journal.pone.0061217

65 Good, I. J. The population frequencies of species and the estimation of population parameters. *Biometrika* **40**, 237-264 (1953). https://doi.org:10.1093/biomet/40.3-4.237

66 Dixon, P. VEGAN, a package of R functions for community ecology. *Journal of Vegetation Science* **14**, 927-930 (2003). https://doi.org:https://doi.org/10.1111/j.1654-1103.2003.tb02228.x

67 Gomez-Lopez, N. *et al.* Inflammasome activation during spontaneous preterm labor with intra-amniotic infection or sterile intra-amniotic inflammation. *Am J Reprod Immunol* **80**, e13049 (2018). https://doi.org:10.1111/aji.13049

68 Romero, R. *et al.* The preterm labor syndrome. *Ann N Y Acad Sci* **734**, 414-429 (1994). https://doi.org:10.1111/j.1749-6632.1994.tb21771.x

69 Norwitz, E. R., Robinson, J. N. & Challis, J. R. The control of labor. *N Engl J Med* **341**, 660-666 (1999). https://doi.org:10.1056/NEJM199908263410906

70 Romero, R. *et al.* The preterm parturition syndrome. *BJOG* **113 Suppl 3**, 17-42 (2006). https://doi.org:10.1111/j.1471-0528.2006.01120.x

71 Smith, R. Parturition. *N Engl J Med* **356**, 271-283 (2007). https://doi.org:10.1056/NEJMra061360

72 Gomez-Lopez, N. *et al.* The immunobiology of preterm labor and birth: intra-amniotic inflammation or breakdown of maternal-fetal homeostasis. *Reproduction* **164**, R11-R45 (2022). https://doi.org:10.1530/REP-22-0046

73 Willcockson, A. R. *et al.* Transcriptome signature identifies distinct cervical pathways induced in lipopolysaccharide-mediated preterm birth. *Biol Reprod* **98**, 408-421 (2018). https://doi.org:10.1093/biolre/iox180

74 Norwitz, E. R. *et al.* Molecular Regulation of Parturition: The Role of the Decidual Clock. *Cold Spring Harb Perspect Med* **5** (2015). https://doi.org:10.1101/cshperspect.a023143

75 Farias-Jofre, M. *et al.* Blockade of IL-6R prevents preterm birth and adverse neonatal outcomes. *EBioMedicine* **98**, 104865 (2023). https://doi.org:10.1016/j.ebiom.2023.104865

76 Saito, H., Sherwood, E. R., Varma, T. K. & Evers, B. M. Effects of aging on mortality, hypothermia, and cytokine induction in mice with endotoxemia or sepsis. *Mech Ageing Dev* **124**, 1047-1058 (2003). https://doi.org:10.1016/j.mad.2003.08.002

77 Copeland, S., Warren, H. S., Lowry, S. F., Calvano, S. E. & Remick, D. Acute inflammatory response to endotoxin in mice and humans. *Clin Diagn Lab Immunol* **12**, 60-67 (2005). https://doi.org:10.1128/cdli.12.1.60-67.2005

78 Migale, R. *et al.* Modeling hormonal and inflammatory contributions to preterm and term labor using uterine temporal transcriptomics. *BMC Med* **14**, 86 (2016). https://doi.org:10.1186/s12916-016-0632-4

79 Pique-Regi, R. *et al.* Single cell transcriptional signatures of the human placenta in term and preterm parturition. *Elife* **8** (2019). https://doi.org:10.7554/eLife.52004

80 Garcia-Flores, V. *et al.* A single-cell atlas of murine reproductive tissues during preterm labor. *Cell Rep*, 111846 (2022). https://doi.org:10.1016/j.celrep.2022.111846

81 Pique-Regi, R. *et al.* A single-cell atlas of the myometrium in human parturition. *JCI Insight* **7** (2022). https://doi.org:10.1172/jci.insight.153921

82 Galaz, J. *et al.* Host-microbiome interactions in distinct subsets of preterm labor and birth. *iScience* **26**, 108341 (2023). https://doi.org:10.1016/j.isci.2023.108341

83 Lavin, Y. & Merad, M. Macrophages: gatekeepers of tissue integrity. *Cancer Immunol Res* **1**, 201-209 (2013). https://doi.org:10.1158/2326-6066.CIR-13-0117

84 Roszer, T. Understanding the Mysterious M2 Macrophage through Activation Markers and Effector Mechanisms. *Mediators Inflamm* **2015**, 816460 (2015). https://doi.org:10.1155/2015/816460

85 Faro, J. *et al.* Intra-amniotic inflammation induces preterm birth by activating the NLRP3 inflammasome. *Biol Reprod* **100**, 1290-1305 (2019). https://doi.org:10.1093/biolre/ioy261

86 Motomura, K. *et al.* The alarmin S100A12 causes sterile inflammation of the human chorioamniotic membranes as well as preterm birth and neonatal mortality in mice. *Biol Reprod* **105**, 1494-1509 (2021). https://doi.org:10.1093/biolre/ioab188

87 Coll, R. C. *et al.* A small-molecule inhibitor of the NLRP3 inflammasome for the treatment of inflammatory diseases. *Nat Med* **21**, 248-255 (2015). https://doi.org:10.1038/nm.3806

88 Gomez de Aguero, M. *et al.* The maternal microbiota drives early postnatal innate immune development. *Science* **351**, 1296-1302 (2016). https://doi.org:10.1126/science.aad2571

89 Lim, A. I. *et al.* Prenatal maternal infection promotes tissue-specific immunity and inflammation in offspring. *Science* **373** (2021). https://doi.org:10.1126/science.abf3002

90 Mirabella, F. *et al.* Prenatal interleukin 6 elevation increases glutamatergic synapse density and disrupts hippocampal connectivity in offspring. *Immunity* **54**, 2611-2631 e2618 (2021). https://doi.org:10.1016/j.immuni.2021.10.006

91 Cuna, A., Morowitz, M. J., Ahmed, I., Umar, S. & Sampath, V. Dynamics of the preterm gut microbiome in health and disease. *Am J Physiol Gastrointest Liver Physiol* **320**, G411-G419 (2021). https://doi.org:10.1152/ajpgi.00399.2020

92 Tamburini, S., Shen, N., Wu, H. C. & Clemente, J. C. The microbiome in early life: implications for health outcomes. *Nat Med* **22**, 713-722 (2016). https://doi.org:10.1038/nm.4142

93 Ficara, M. *et al.* Changes of intestinal microbiota in early life. *J Matern Fetal Neonatal Med* **33**, 1036-1043 (2020). https://doi.org:10.1080/14767058.2018.1506760

94 Puri, K. *et al.* Association of Chorioamnionitis with Aberrant Neonatal Gut Colonization and Adverse Clinical Outcomes. *PLoS One* **11**, e0162734 (2016). https://doi.org:10.1371/journal.pone.0162734

95 Mitchell, B. F. & Taggart, M. J. Are animal models relevant to key aspects of human parturition? *Am J Physiol Regul Integr Comp Physiol* **297**, R525-545 (2009). https://doi.org:10.1152/ajpregu.00153.2009

96 Soncin, F., Natale, D. & Parast, M. M. Signaling pathways in mouse and human trophoblast differentiation: a comparative review. *Cell Mol Life Sci* **72**, 1291-1302 (2015). https://doi.org:10.1007/s00018-014-1794-x

97 McCarthy, R. *et al.* Mouse models of preterm birth: suggested assessment and reporting guidelines. *Biol Reprod* **99**, 922-937 (2018). https://doi.org:10.1093/biolre/ioy109

Figure Legends

Figure 1. M2 macrophages prevent HMGB1-induced preterm birth and neonatal mortality. **a** To mimic the clinical condition of sterile intra-amniotic inflammation (SIAI), the alarmin HMGB1 was intra-amniotically administered to C57BL/6 dams under ultrasound guidance on 14.5 days *post coitum* (dpc). Bone marrow-derived cells were collected from C57BL/6 mice, differentiated, and polarized to an M2 phenotype (M2 MΦ) *in vitro*. M2 MΦ were administered intravenously to C57BL/6 dams on 13.5 and 14.5 dpc. Dams were monitored until delivery, and neonatal survival and weight were recorded until three weeks of age. **b** Gestational length shown as box plots where midlines indicate medians and whiskers indicate minimum/maximum range. P-values were determined using the Kruskal-Wallis test followed by two-stage linear step-up procedure of Benjamini, Krieger, and Yekutieli post-hoc test. **c** Rates of preterm birth among dams injected with PBS (n = 20), HMGB1 (n = 28), PBS + M2 MΦ (n = 14), and HMGB1 + M2 MΦ (n = 29) are shown as bar plots. P-values were determined using Fisher's exact test. **d** Pie charts representing the survival at birth of preterm neonates. PBS (n = 20 litters), HMGB1 (n = 20 litters), PBS + M2 MΦ (n = 14 litters), and HMGB1 + M2 MΦ (n = 16 litters). **e** Kaplan-Meier survival curves from neonates at weeks 1, 2, and 3 of life. PBS (n = 20 litters), HMGB1 (n = 20 litters), PBS + M2 MΦ (n = 14 litters), and HMGB1 + M2 MΦ (n = 16 litters). P-values were determined using the Gehan-Breslow-Wilcoxon test. **f** Individual weights (grams, g) of neonates across the first three weeks of life are shown as box plots where midlines indicate medians and whiskers indicate minimum/maximum range. PBS (n = 11 litters), HMGB1 (n = 11 litters), PBS + M2 MΦ (n = 11 litters), and HMGB1 + M2 MΦ (n = 14 litters). P-values were determined using the Kruskal-Wallis test followed by Dunn's post-hoc test. *$p < 0.05$; **$p < 0.01$; ***$p < 0.001$.

Figure 2. M2 macrophages dampen HMGB1-induced inflammation, including inflammasome activation, in the amniotic cavity. a Dams were intra-amniotically injected with HMGB1 on 14.5 days *post coitum* (dpc). Amniotic fluid was collected at 24, 48, 72, or 96 h post-HMGB1 injection for cytokine determination. **b** Concentrations of IL-6 in the amniotic fluid of HMGB1-injected dams at 24, 48, 72, and 96 h post-injection are shown as box plots (n = 8 dams per time point). P-values were determined using the Kruskal-Wallis test followed by two-stage linear step-up procedure of Benjamini, Krieger, and Yekutieli post-hoc test. **c** M2 macrophages (M2 MΦ) or vehicle (PBS) were intravenously administered on 13.5 dpc and 14.5 dpc to dams followed by ultrasound-guided intra-amniotic injection of HMGB1 on 14.5 dpc. Amniotic fluid was collected at 72 h post-HMGB1 injection for cytokine determination. **d** Concentrations of IL-6, TNF, and total IL-1β in the amniotic fluid of the HMGB1+Vehicle dams (n = 16 dams) or HMGB1+M2 MΦ dams (n = 16 dams) at 72 h post-injection are shown as box plots. P-values were determined using the Mann-Whitney U-test. **e** To determine inflammasome activation, amniotic fluid of dams that received PBS, HMGB1, HMGB1 + Vehicle, or HMGB1 + M2 MΦ was collected at 72 h post-HMGB1 injection for immunoblotting. **f** Immunoblotting of active caspase (CASP)-1 expression and mature IL-1β expression in the amniotic fluid of dams injected with PBS or HMGB1. Representative CASP-1 immunoblot image shows 6 samples per group, and representative mature IL-1β immunoblot image shows 3 pooled samples (pooled amniotic fluids from 3 dams) per group. **g** Protein quantification of active CASP-1 in the amniotic fluid of dams injected with PBS (n = 12) or HMGB1 (n = 13). Protein quantification of mature IL-1β in the pooled amniotic fluid of dams injected with PBS (n = 3) or HMGB1 (n = 3). Data are shown as boxplots where midlines indicate medians, boxes denote interquartile ranges, and whiskers indicate the minimum/maximum range. P-values were determined using the Mann-Whitney U-test

or t-test. **h** Immunoblotting of active CASP-1 expression and mature IL-1β expression in the amniotic fluid of HMGB1+Vehicle or HMGB1+M2 MΦ dams. Representative CASP-1 immunoblot image shows 6 samples per group, and representative mature IL-1β immunoblot image shows 3 pooled samples (pooled amniotic fluids from 3 dams) per group. **i** Protein quantification of active CASP-1 in the amniotic fluid of dams injected with HMGB1+Vehicle (n = 12) or HMGB1+M2 MΦ (n = 14). Protein quantification of mature IL-1β in the pooled amniotic fluid of dams injected with HMGB1+Vehicle (n = 3) or HMGB1+M2 MΦ (n = 3). P-values were determined using the Mann-Whitney U-test or t-test. Data are shown as boxplots where midlines indicate medians, boxes denote interquartile ranges, and whiskers indicate the minimum/maximum range. *p < 0.05; **p < 0.01; ***p < 0.001.

Figure 3. M2 macrophages inhibit inflammasome activation and regulate gene expression in the fetal membranes. a Dams received intra-amniotic injection of PBS (control) or HMGB1 on 14.5 days *post coitum* (dpc). M2-polarized macrophages (M2 MΦ) or vehicle (PBS) were intravenously administered to dams on 13.5 dpc and 14.5 dpc followed by intra-amniotic injection of HMGB1 on 14.5 dpc. Tissue collection was performed at 72 h post-injection to collect the fetal membranes for immunoblotting and to determine gene expression. **b** Immunoblotting of active caspase (CASP)-1, mature IL-1β, and β-actin (ACTB) in the fetal membranes of PBS- or HMGB1-injected dams. Representative immunoblot images depict 6 samples per group in each gel. **c** Protein quantification of active CASP-1 and mature IL-1β (both normalized by ACTB) in the fetal membranes of PBS- or HMGB1-injected dams (n = 6 per group). **d** Immunoblotting of active CASP-1, mature IL-1β, and ACTB in the fetal membranes from HMGB1+Vehicle or HMGB1+M2 MΦ dams. Representative immunoblot images depict 6 samples per group in each

gel. **e** Relative quantification of active CASP-1 and mature IL-1β (both normalized by ACTB) in the fetal membranes of HMGB1+Vehicle or HMGB1+M2 MΦ dams (n = 6 per group). **f** Representative heatmaps displaying the expression of key inflammatory genes in the fetal membranes of PBS- (n = 8) or HMGB1-injected (n = 8) dams. **g** Expression of *Ccl17* in the fetal membranes of PBS- or HMGB1-injected dams. Data are shown as boxplots where midlines indicate medians, boxes denote interquartile ranges, and whiskers indicate the minimum/maximum range. P-values were determined using the Mann-Whitney U-test. **h** Representative heatmaps displaying the expression of key inflammatory genes in the fetal membranes of HMGB1+Vehicle (n = 8) or HMGB1+M2 MΦ (n = 8) dams. **i** Expression of *Tlr4*, *Cxcl1*, *Tnf*, and *Il1b* in the fetal membranes of HMGB1+Vehicle or HMGB1+M2 MΦ dams. Data are shown as boxplots where midlines indicate medians, boxes denote interquartile ranges, and whiskers indicate the minimum/maximum range. P-values were determined using the Mann-Whitney U-test. *$p < 0.05$; **$p < 0.01$.

Figure 4. Adoptively transferred M2 macrophages reach intrauterine compartments. a Bone marrow-derived cells were collected from donor CD45.1^{+} mice, differentiated, and polarized to M2 MΦ *in vitro*. Donor M2 MΦ were intravenously administered on 13.5 days *post coitum* (dpc) and 14.5 dpc to recipient CD45.2^{+} dams followed by intra-amniotic injection of HMGB1 on 14.5 dpc. Maternal and fetal tissues were collected at 2, 6, or 12 h post-HMGB1 injection (n = 3 dams per time point) to track donor M2 macrophage infiltration. **b** Representative gating strategy for detection of live CD45.1^{+}F4/80^{+} or CD45.2^{+}F4/80^{+} cells. **c** Representative flow cytometry plots to detect CD45.1^{+}CD45.2^{-} donor macrophages in the maternal blood, maternal lung, uterus, decidua, placenta, fetal membrane, and amniotic fluid of recipient dams at 2 (top row), 6 (middle row), or

12 (bottom row) h post-HMGB1 injection. Proportions of donor macrophages are shown in the bottom right corner of each plot. **d** Quantification of donor M2 macrophages ($F4/80^+CD45.1^+$ cells) in the maternal tissues of recipient dams collected at 2, 6, or 12 h post-HMGB1 injection (n = 3 dams per time point). **e** Quantification of donor M2 macrophages ($F4/80^+CD45.1^+$ cells) in the placenta, fetal membranes, and amniotic fluid of recipient dams collected at 2, 6, or 12 h post-HMGB1 injection (n = 3 dams per time point). Data are presented as violin plots where the midline represents the median, dotted lines represent the interquartile range (IQR), and whiskers represent the minimum/maximum range. P-values were determined using the Kruskal-Wallis test followed by Dunn's post-hoc test. *$p < 0.05$.

Figure 5. M2 macrophages ameliorate fetal and neonatal lung inflammation induced by *in utero* exposure to HMGB1. a Dams received intra-amniotic injection of PBS (control) or HMGB1 on 14.5 days *post coitum* (dpc). M2-polarized macrophages (M2 MΦ) or vehicle (PBS) were intravenously administered to dams on 13.5 dpc and 14.5 dpc followed by intra-amniotic injection of HMGB1 on 14.5 dpc. Tissue collection was performed at 72 h post-injection to collect the fetal lung for gene expression. **b** Representative heatmaps displaying the expression of inflammatory genes in the fetal lung of PBS- (n = 8) or HMGB1-injected (n = 8) dams. **c** Expression of *Il6*, *Tnfrsf1a*, *Il33*, *Nlrp6*, and *Tlr9* in the fetal lung of PBS- or HMGB1-injected dams. Data are shown as boxplots where midlines indicate medians, boxes denote interquartile ranges, and whiskers indicate the minimum/maximum range. P-values were determined using the Mann-Whitney U-test. **d** Representative heatmaps displaying the expression of inflammatory genes in the fetal lung of HMGB1+Vehicle (n = 8) or HMGB1+M2 MΦ (n = 8) dams. **e** Expression of *Tnfrsf1a* and *Nod1* in the fetal lung of HMGB1+Vehicle or HMGB1+M2 MΦ dams. **f** The lung

was collected at 14-16 days of life from neonates born to HMGB1+Vehicle or HMGB1+M2 MΦ dams to evaluate gene expression as shown in the representative heatmap. **g** Expression of *Il6*, *Ccl2*, *Socs3*, and *Cxcl1* in the neonatal lung (n = 10 per group). Data are shown as boxplots where midlines indicate medians, boxes denote interquartile ranges, and whiskers indicate the minimum/maximum range. P-values were determined using the Mann-Whitney U-test. *$p < 0.05$; **$p < 0.01$.

Figure 6. M2 macrophages regulate neonatal gut inflammation resulting from *in utero* exposure to HMGB1. a M2 macrophages (M2 MΦ) or PBS (Vehicle) were intravenously administered to dams on 13.5 dpc and 14.5 dpc followed by intra-amniotic injection of HMGB1 on 14.5 dpc. After delivery, neonates were monitored until 14-16 days of age, after which the small intestine, cecum, and colon were collected to determine gene expression. Representative heatmaps display gene expression in the **b** neonatal small intestine, **d** cecum, and **f** colon of neonates born to HMGB1+Vehicle (n = 10 neonates) or HMGB1+M2 MΦ (n = 10 neonates) dams. The expression of specific genes in the **c** neonatal small intestine (*Aim2, Cd68, Tnf, Rgs4, Ccl5, Ccl17*), **e** cecum (*Casp1* and *Ccl17*), and **g** colon (*Il1a, Cd68, Casp1, Jun, Kdm6b, Ccl17*) are shown as box plots. P-values were determined using the Mann-Whitney U-test. Data are shown as boxplots where midlines indicate medians, boxes denote interquartile ranges, and whiskers indicate the minimum/maximum range. *$p < 0.05$; **$p < 0.01$.

Figure 7. M2 macrophages modulate neonatal gut microbiome dysbiosis resulting from *in utero* exposure to HMGB1. a M2 macrophages (M2 MΦ) or PBS (Vehicle) were intravenously administered to dams on 13.5 dpc and 14.5 dpc followed by intra-amniotic injection of HMGB1

on 14.5 dpc. After delivery, neonates were monitored until 14-16 days of age, after which the small intestine, cecum, and colon were collected for microbial analysis using 16S rRNA gene sequencing (n = 10 neonates per group). Principal coordinates analysis (PCoA) illustrating variation in the 16S rRNA gene profiles among the **b** small intestine, **e** cecum, and **h** colon. Similarities in the 16S rRNA gene profiles were characterized using the Bray-Curtis similarity index. Bar plots showing the taxonomic classifications of the 20 bacterial taxa with highest relative abundance across all **c** small intestine, **f** cecum, and **i** colon samples. Multiple taxa with the same bacterial taxonomic classification within a same sample are indicated by bars of the same color. Changes in abundance of **d** *Rodentibacter* (ASV-5) and *Ruminiclostridium* (ASV-17) in the neonatal small intestine, **g** *Ruminiclostridium* (ASV-17), *Lachnospiraceae* (ASV-24), *Lachnoclostridium* (ASV-15), and *Lachnospiraceae* (ASV-39) in the neonatal cecum, and **j** *Ruminiclostridium* (ASV-17), *Lachnospiraceae* (ASV-24), and *Lachnoclostridium* (ASV-15) in the neonatal colon. Data are shown as box plots where midlines indicate medians, boxes denote interquartile ranges, and whiskers indicate the minimum/maximum range. P-values were determined using Mann-Whitney U-tests with Holm's correction for multiple comparisons. #q < 0.1.

Figure 8. M2 macrophages improve neonatal immunocompetence following *in utero* exposure to HMGB1. a M2 macrophages (M2 MΦ) or PBS (Vehicle) were intravenously administered to dams on 13.5 dpc and 14.5 dpc followed by intra-amniotic injection of HMGB1 on 14.5 dpc. Pregnant dams without any treatment or injected with HMGB1 alone were also included. After delivery, surviving neonates were monitored until 14-16 days of age, after which they received intraperitoneal injection of Group B *Streptococcus* (GBS) and were observed for five days. **b** The survival rates of GBS-infected neonates born to untreated (n = 10 neonates),

HMGB1-injected (n = 10 neonates), HMGB1+Vehicle (n = 12 neonates), or HMGB1+M2 MΦ (n = 12 neonates) dams over the five days post-challenge are displayed as Kaplan-Meier survival curves. P-values were determined using the Gehan-Breslow-Wilcoxon test. **c** Mean weights of GBS-infected neonates over the five days post-challenge. P-values for comparing the mean weight at the end of day five (final data point in plot) were determined using the Mann-Whitney U-test. *$p < 0.05$; **$p < 0.01$; ***$p < 0.001$.

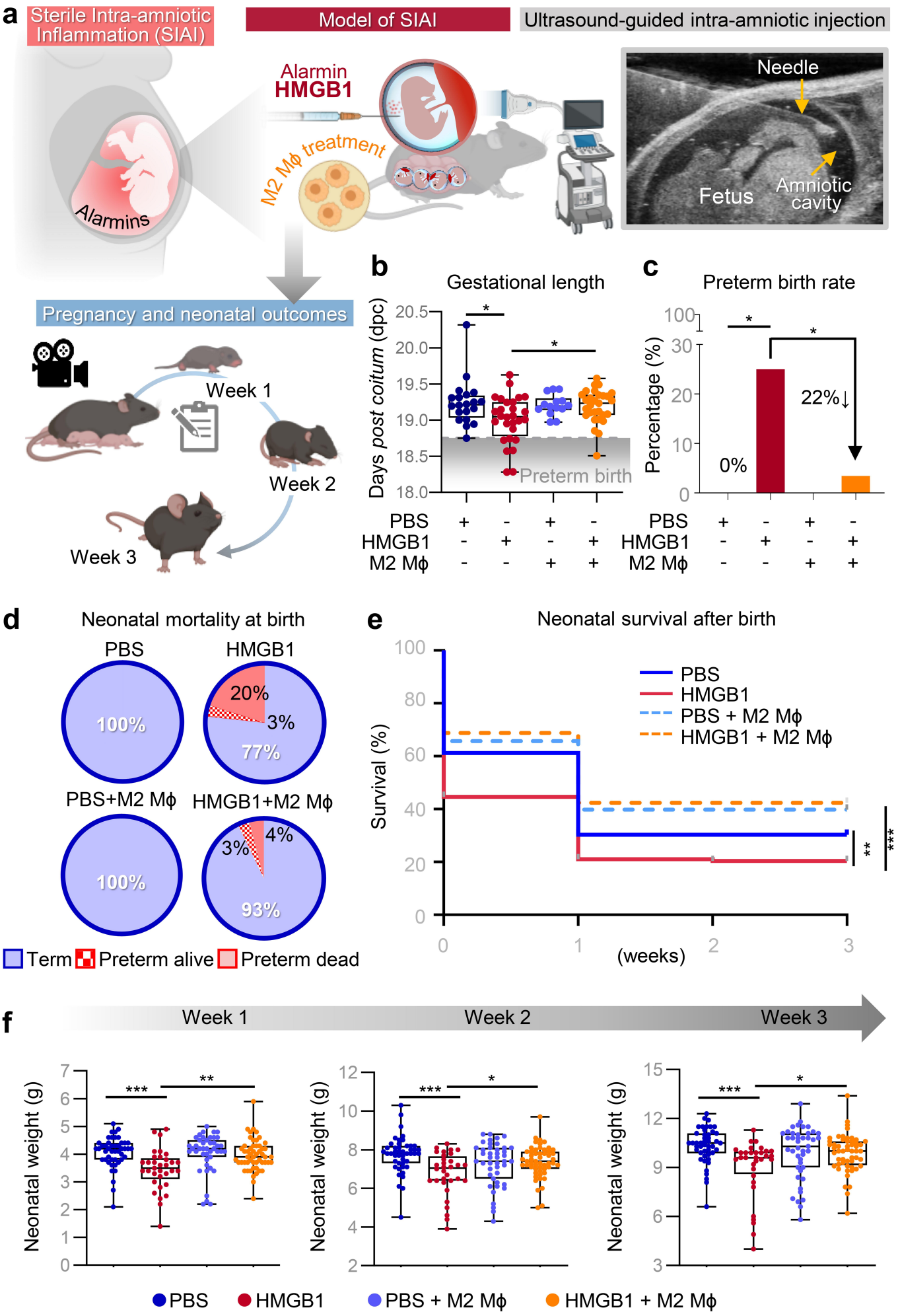
a
Sterile Intra-amniotic Inflammation (SIAI)
Model of SIAI
Ultrasound-guided intra-amniotic injection
Alarmin
HMGB1
M2 Mϕ treatment
Alarmins
Needle
Fetus
Amniotic cavity
Pregnancy and neonatal outcomes
Week 1
Week 2
Week 3
b
Gestational length
Days post coitum (dpc)
Preterm birth
PBS
HMGB1
M2 Mϕ
c
Preterm birth rate
Percentage (%)
0%
22%↓
d
Neonatal mortality at birth
PBS
HMGB1
PBS+M2 Mϕ
HMGB1+M2 Mϕ
100%
20%
3%
77%
4%
93%
Term
Preterm alive
Preterm dead
e
Neonatal survival after birth
Survival (%)
(weeks)
PBS
HMGB1
PBS + M2 Mϕ
HMGB1 + M2 Mϕ
f
Week 1
Week 2
Week 3
Neonatal weight (g)
PBS
HMGB1
PBS + M2 Mϕ
HMGB1 + M2 Mϕ

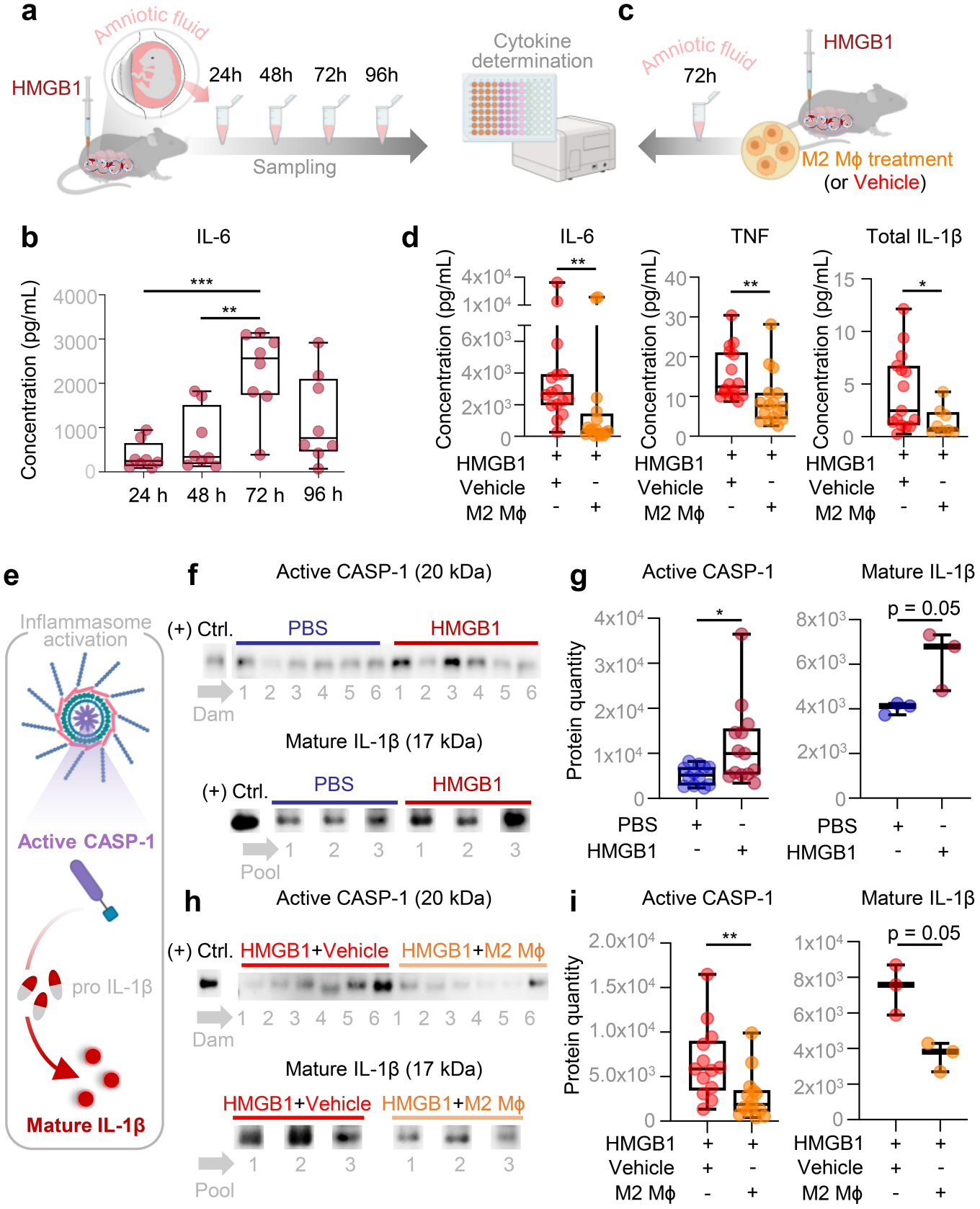
a
Amniotic fluid
HMGB1
24h 48h 72h 96h
Sampling
Cytokine determination
c
Amniotic fluid
72h
HMGB1
M2 Mϕ treatment
(or Vehicle)
b
IL-6
Concentration (pg/mL)
4000
3000
2000
1000
0
***
**
24 h 48 h 72 h 96 h
d
IL-6
TNF
Total IL-1β
Concentration (pg/mL)
4x10⁴
1x10⁴
6x10³
4x10³
2x10³
0
40
30
20
10
15
5
**
*
HMGB1 + +
Vehicle + -
M2 Mϕ - +
e
Inflammasome activation
Active CASP-1
pro IL-1β
Mature IL-1β
f
Active CASP-1 (20 kDa)
(+) Ctrl.
PBS
HMGB1
1 2 3 4 5 6 1 2 3 4 5 6
Dam
Mature IL-1β (17 kDa)
(+) Ctrl.
PBS
HMGB1
1 2 3 1 2 3
Pool
g
Active CASP-1
Mature IL-1β
Protein quantity
4x10⁴
3x10⁴
2x10⁴
1x10⁴
0
8x10³
6x10³
4x10³
2x10³
0
*
p = 0.05
PBS + -
HMGB1 - +
h
Active CASP-1 (20 kDa)
(+) Ctrl.
HMGB1+Vehicle
HMGB1+M2 Mϕ
1 2 3 4 5 6 1 2 3 4 5 6
Dam
Mature IL-1β (17 kDa)
HMGB1+Vehicle
HMGB1+M2 Mϕ
1 2 3 1 2 3
Pool
i
Active CASP-1
Mature IL-1β
Protein quantity
2.0x10⁴
1.5x10⁴
1.0x10⁴
5.0x10³
0
1x10⁴
8x10³
6x10³
4x10³
2x10³
0
**
p = 0.05
HMGB1 + +
Vehicle + -
M2 Mϕ - +

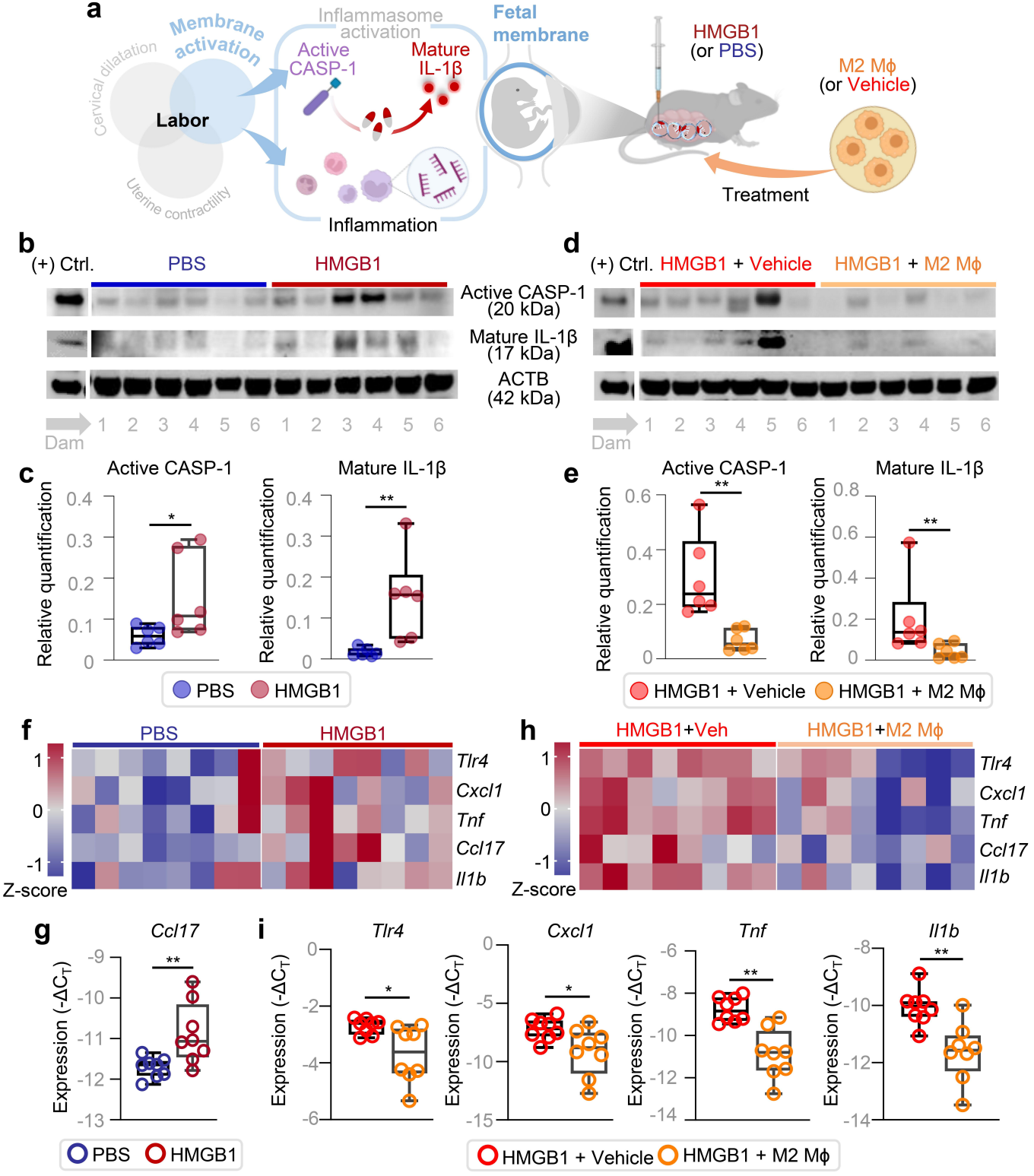
a
Membrane activation
Cervical dilatation
Labor
Uterine contractility
Inflammasome activation
Active CASP-1
Mature IL-1β
Inflammation
Fetal membrane
HMGB1 (or PBS)
M2 Mϕ (or Vehicle)
Treatment
b
(+) Ctrl.
PBS
HMGB1
Active CASP-1 (20 kDa)
Mature IL-1β (17 kDa)
ACTB (42 kDa)
Dam
1 2 3 4 5 6 1 2 3 4 5 6
d
(+) Ctrl.
HMGB1 + Vehicle
HMGB1 + M2 Mϕ
Dam
1 2 3 4 5 6 1 2 3 4 5 6
c
Active CASP-1
Mature IL-1β
Relative quantification
PBS
HMGB1
e
Active CASP-1
Mature IL-1β
Relative quantification
HMGB1 + Vehicle
HMGB1 + M2 Mϕ
f
PBS
HMGB1
Tlr4
Cxcl1
Tnf
Ccl17
Il1b
Z-score
h
HMGB1+Veh
HMGB1+M2 Mϕ
Tlr4
Cxcl1
Tnf
Ccl17
Il1b
Z-score
g
Ccl17
Expression (-ΔCT)
PBS
HMGB1
i
Tlr4
Cxcl1
Tnf
Il1b
Expression (-ΔCT)
HMGB1 + Vehicle
HMGB1 + M2 Mϕ

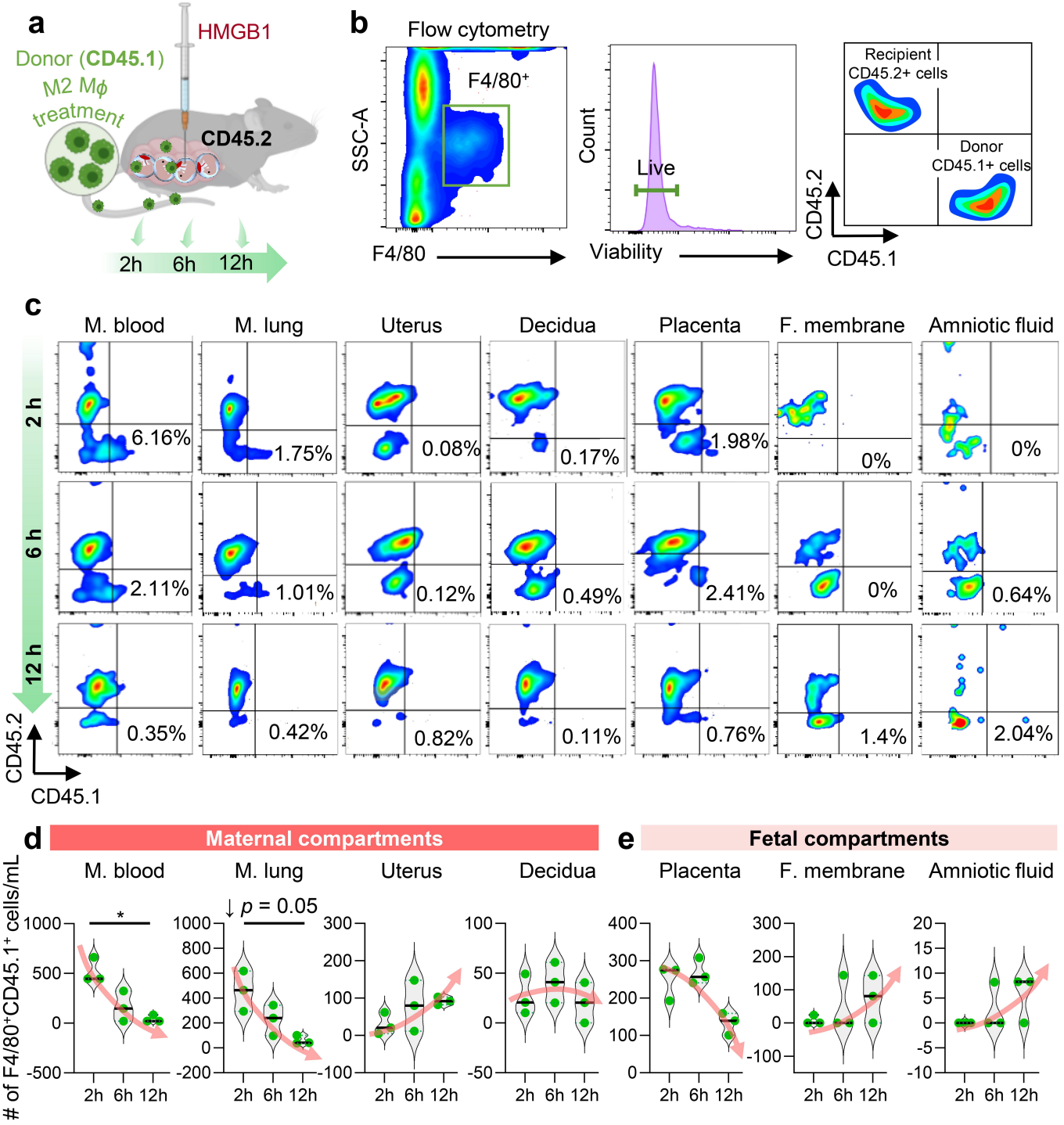
a
HMGB1
Donor (CD45.1)
M2 Mϕ
treatment
CD45.2
2h
6h
12h
b
Flow cytometry
F4/80+
SSC-A
F4/80
Count
Live
Viability
Recipient
CD45.2+ cells
Donor
CD45.1+ cells
CD45.2
CD45.1
c
M. blood
M. lung
Uterus
Decidua
Placenta
F. membrane
Amniotic fluid
2 h
6 h
12 h
6.16%
1.75%
0.08%
0.17%
1.98%
0%
0%
2.11%
1.01%
0.12%
0.49%
2.41%
0%
0.64%
0.35%
0.42%
0.82%
0.11%
0.76%
1.4%
2.04%
CD45.2
CD45.1
d
Maternal compartments
M. blood
M. lung
Uterus
Decidua
p = 0.05
*
# of F4/80+CD45.1+ cells/mL
2h
6h
12h
e
Fetal compartments
Placenta
F. membrane
Amniotic fluid

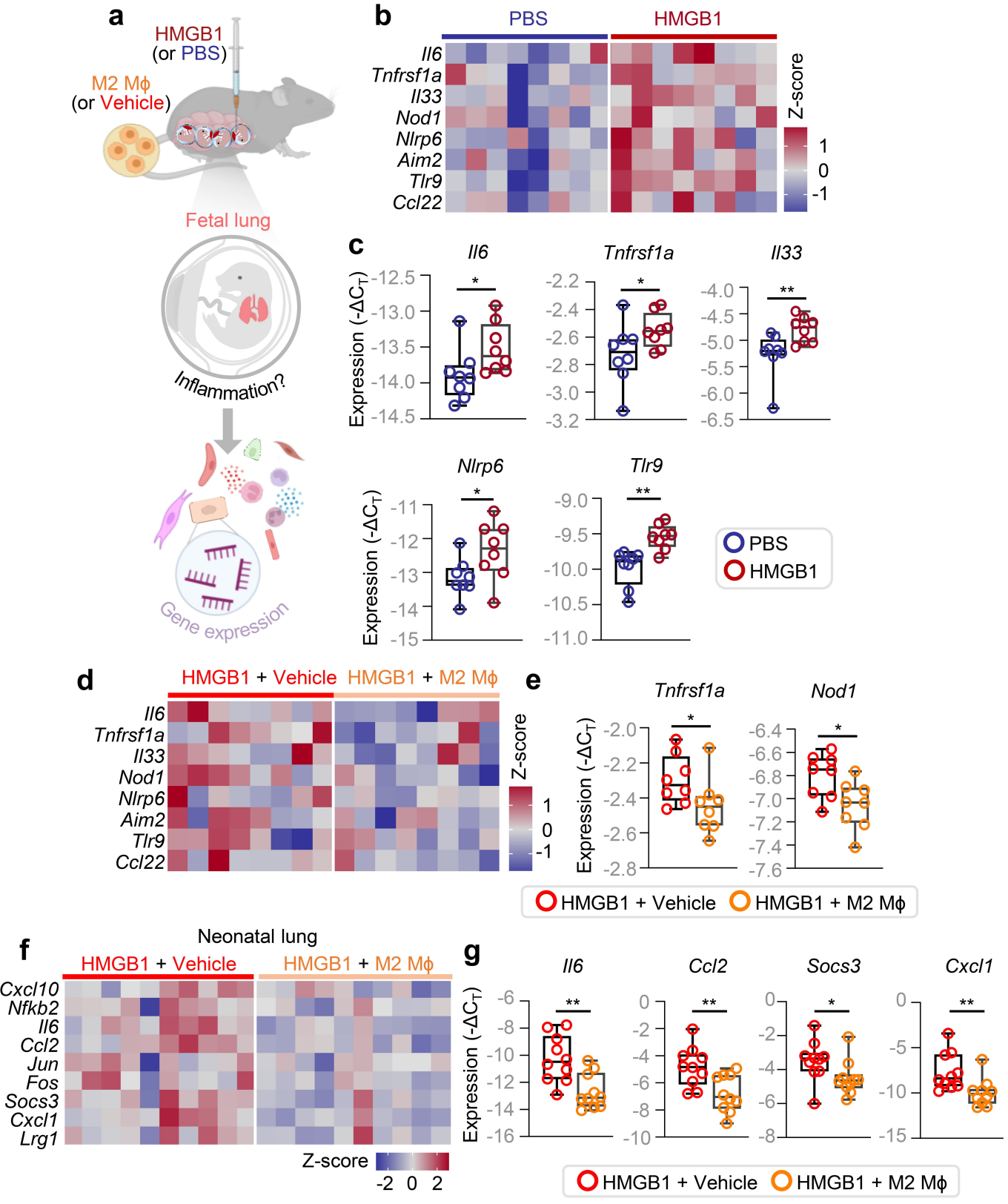
a
HMGB1
(or PBS)
M2 Mϕ
(or Vehicle)
Fetal lung
Inflammation?
Gene expression
b
PBS
HMGB1
Il6
Tnfrsf1a
Il33
Nod1
Nlrp6
Aim2
Tlr9
Ccl22
Z-score
1
0
-1
c
Il6
Tnfrsf1a
Il33
Nlrp6
Tlr9
Expression (-ΔC_T)
PBS
HMGB1
d
HMGB1 + Vehicle
HMGB1 + M2 Mϕ
Il6
Tnfrsf1a
Il33
Nod1
Nlrp6
Aim2
Tlr9
Ccl22
Z-score
1
0
-1
e
Tnfrsf1a
Nod1
Expression (-ΔC_T)
HMGB1 + Vehicle
HMGB1 + M2 Mϕ
f
Neonatal lung
HMGB1 + Vehicle
HMGB1 + M2 Mϕ
Cxcl10
Nfkb2
Il6
Ccl2
Jun
Fos
Socs3
Cxcl1
Lrg1
Z-score
-2
0
2
g
Il6
Ccl2
Socs3
Cxcl1
Expression (-ΔC_T)
HMGB1 + Vehicle
HMGB1 + M2 Mϕ

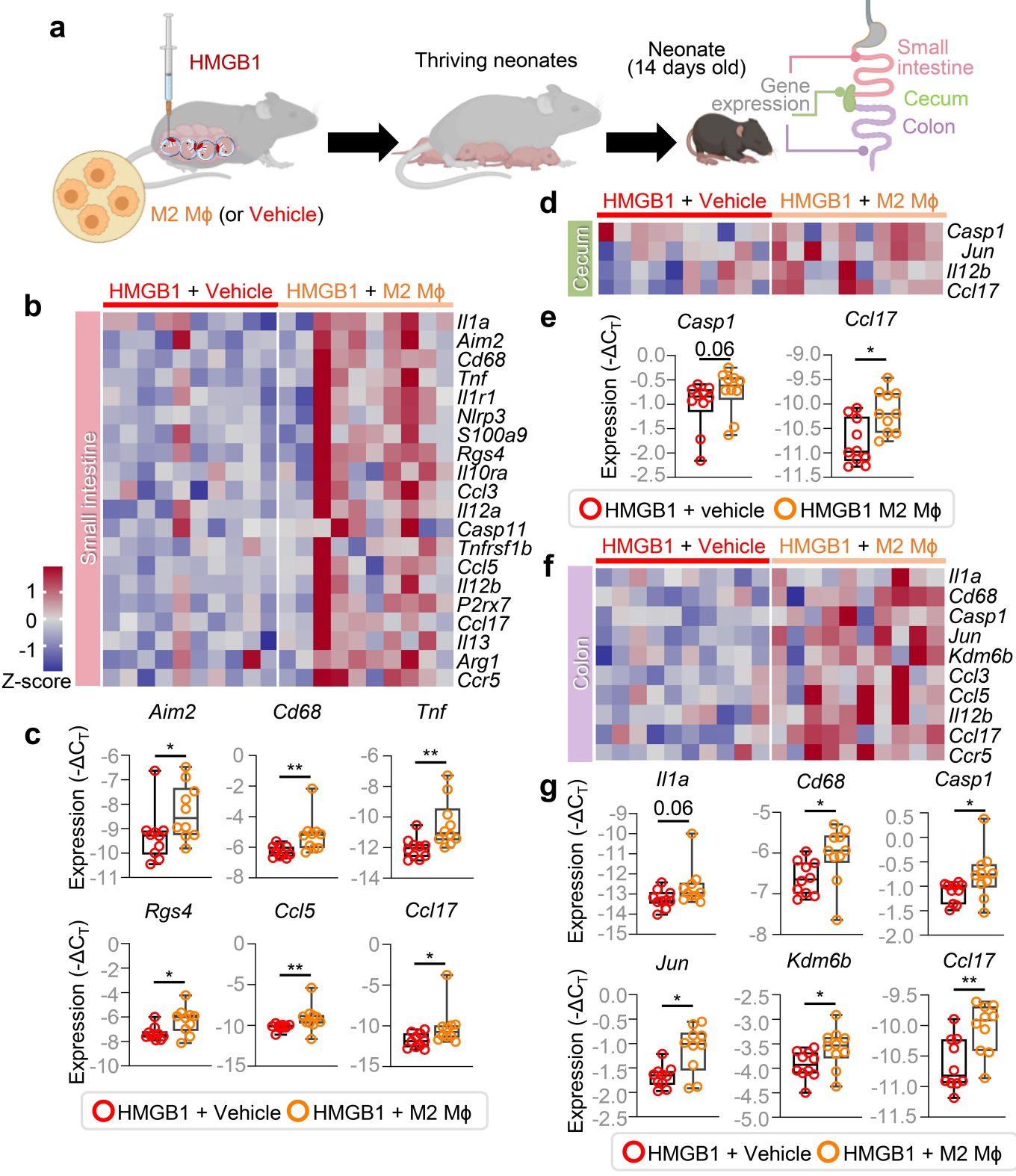
a
HMGB1
M2 Mϕ (or Vehicle)
Thriving neonates
Neonate
(14 days old)
Gene
expression
Small
intestine
Cecum
Colon
b
HMGB1 + Vehicle
HMGB1 + M2 Mϕ
Small intestine
Il1a
Aim2
Cd68
Tnf
Il1r1
Nlrp3
S100a9
Rgs4
Il10ra
Ccl3
Il12a
Casp11
Tnfrsf1b
Ccl5
Il12b
P2rx7
Ccl17
Il13
Arg1
Ccr5
1
0
-1
Z-score
c
Aim2
Cd68
Tnf
Rgs4
Ccl5
Ccl17
Expression (-ΔCT)
HMGB1 + Vehicle
HMGB1 + M2 Mϕ
d
HMGB1 + Vehicle
HMGB1 + M2 Mϕ
Cecum
Casp1
Jun
Il12b
Ccl17
e
Casp1
Ccl17
0.06
Expression (-ΔCT)
HMGB1 + vehicle
HMGB1 M2 Mϕ
f
HMGB1 + Vehicle
HMGB1 + M2 Mϕ
Colon
Il1a
Cd68
Casp1
Jun
Kdm6b
Ccl3
Ccl5
Il12b
Ccl17
Ccr5
g
Il1a
Cd68
Casp1
Jun
Kdm6b
Ccl17
0.06
Expression (-ΔCT)
HMGB1 + Vehicle
HMGB1 + M2 Mϕ

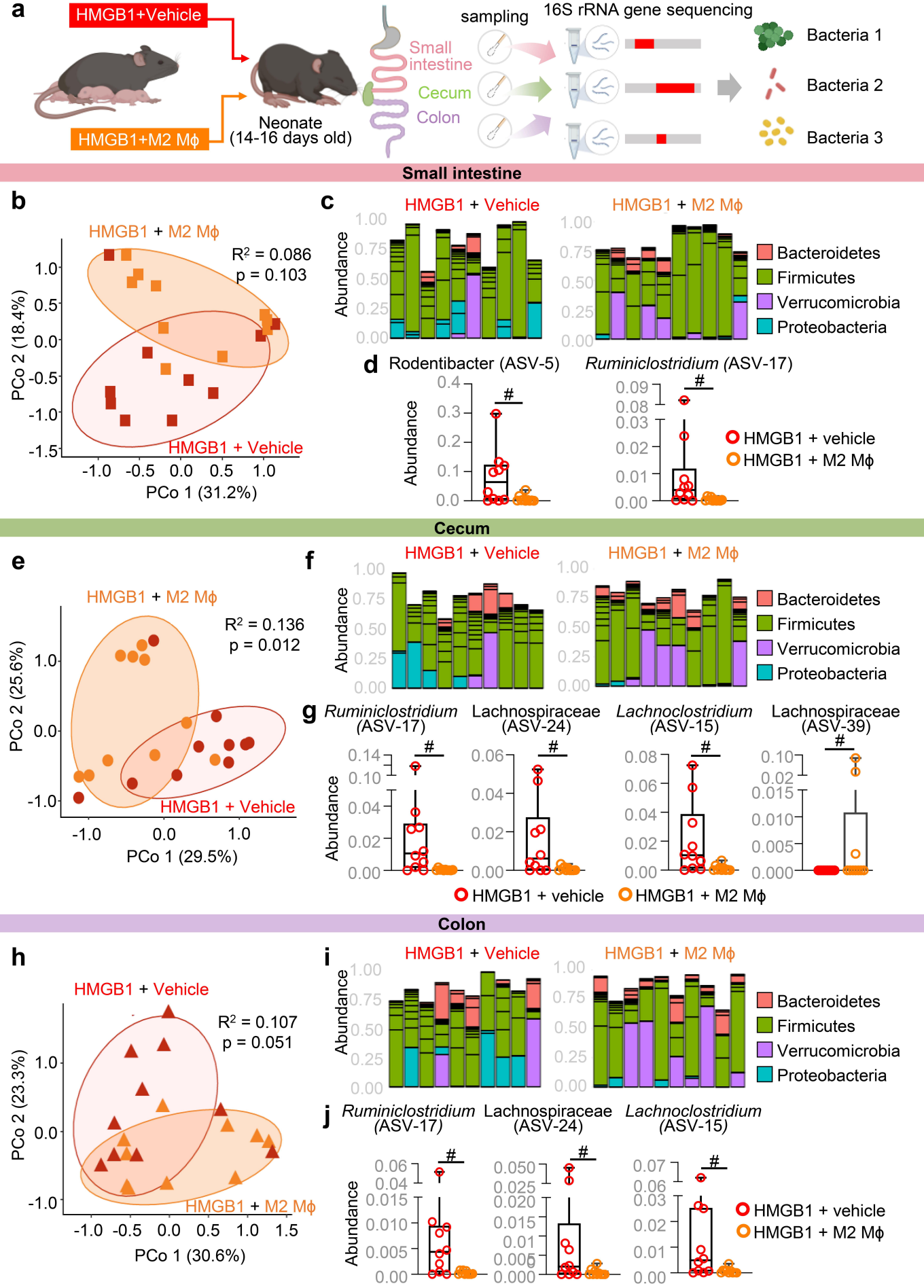
a
HMGB1+Vehicle
HMGB1+M2 Mϕ
Neonate
(14-16 days old)
Small intestine
Cecum
Colon
sampling
16S rRNA gene sequencing
Bacteria 1
Bacteria 2
Bacteria 3
Small intestine
b
HMGB1 + M2 Mϕ
R² = 0.086
p = 0.103
HMGB1 + Vehicle
PCo 2 (18.4%)
PCo 1 (31.2%)
c
HMGB1 + Vehicle
HMGB1 + M2 Mϕ
Abundance
Bacteroidetes
Firmicutes
Verrucomicrobia
Proteobacteria
d
Rodentibacter (ASV-5)
Ruminiclostridium (ASV-17)
Abundance
HMGB1 + vehicle
HMGB1 + M2 Mϕ
Cecum
e
HMGB1 + M2 Mϕ
R² = 0.136
p = 0.012
HMGB1 + Vehicle
PCo 2 (25.6%)
PCo 1 (29.5%)
f
HMGB1 + Vehicle
HMGB1 + M2 Mϕ
Abundance
Bacteroidetes
Firmicutes
Verrucomicrobia
Proteobacteria
g
Ruminiclostridium (ASV-17)
Lachnospiraceae (ASV-24)
Lachnoclostridium (ASV-15)
Lachnospiraceae (ASV-39)
Abundance
HMGB1 + vehicle
HMGB1 + M2 Mϕ
Colon
h
HMGB1 + Vehicle
R² = 0.107
p = 0.051
HMGB1 + M2 Mϕ
PCo 2 (23.3%)
PCo 1 (30.6%)
i
HMGB1 + Vehicle
HMGB1 + M2 Mϕ
Abundance
Bacteroidetes
Firmicutes
Verrucomicrobia
Proteobacteria
j
Ruminiclostridium (ASV-17)
Lachnospiraceae (ASV-24)
Lachnoclostridium (ASV-15)
Abundance
HMGB1 + vehicle
HMGB1 + M2 Mϕ

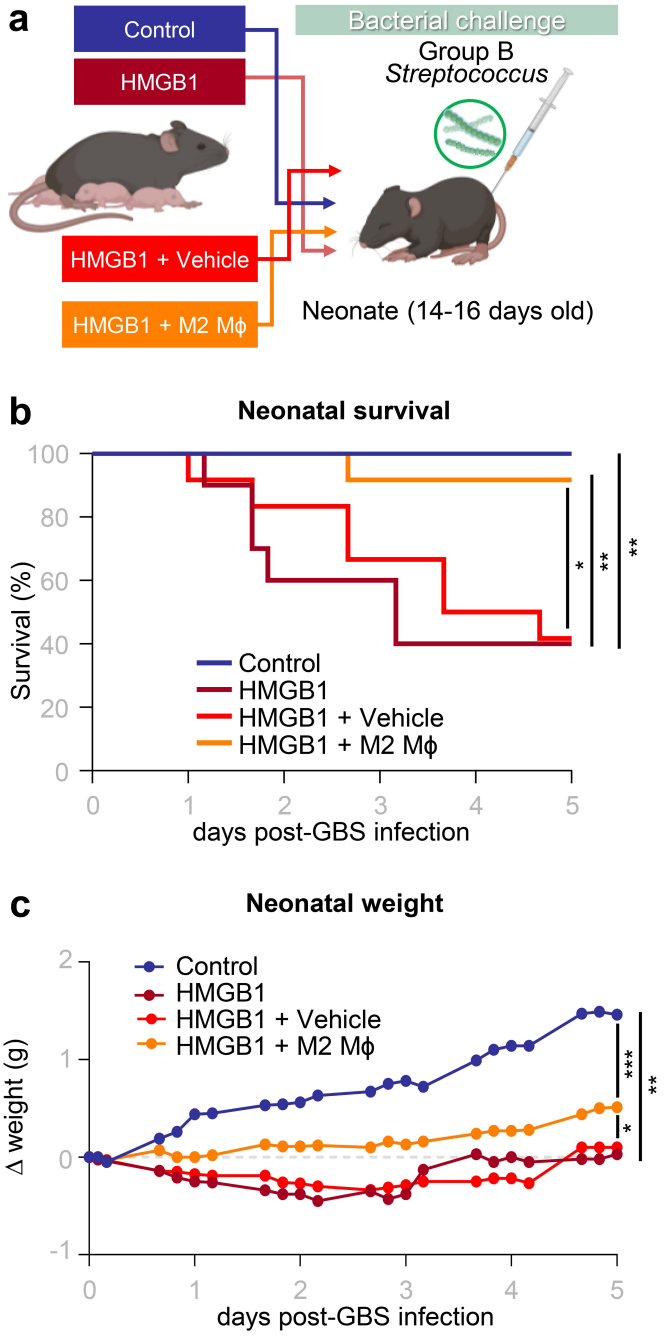
a
Control
HMGB1
HMGB1 + Vehicle
HMGB1 + M2 Mϕ
Bacterial challenge
Group B
Streptococcus
Neonate (14-16 days old)
b
Neonatal survival
Survival (%)
100
80
60
40
20
0
Control
HMGB1
HMGB1 + Vehicle
HMGB1 + M2 Mϕ
*
**
**
0
1
2
3
4
5
days post-GBS infection
c
Neonatal weight
Δ weight (g)
2
1
0
-1
Control
HMGB1
HMGB1 + Vehicle
HMGB1 + M2 Mϕ
***
*
**
0
1
2
3
4
5
days post-GBS infection